

Vecchia-approximated Deep Gaussian Processes for Computer Experiments

Annie Sauer*

Andrew Cooper[†]

Robert B. Gramacy[†]

August 16, 2022

Abstract

Deep Gaussian processes (DGPs) upgrade ordinary GPs through functional composition, in which intermediate GP layers warp the original inputs, providing flexibility to model non-stationary dynamics. Two DGP regimes have emerged in recent literature. A “big data” regime, prevalent in machine learning, favors approximate, optimization-based inference for fast, high-fidelity prediction. A “small data” regime, preferred for computer surrogate modeling, deploys posterior integration for enhanced uncertainty quantification (UQ). We aim to bridge this gap by expanding the capabilities of Bayesian DGP posterior inference through the incorporation of the Vecchia approximation, allowing linear computational scaling without compromising accuracy or UQ. We are motivated by surrogate modeling of simulation campaigns with upwards of 100,000 runs – a size too large for previous fully-Bayesian implementations – and demonstrate prediction and UQ superior to that of “big data” competitors. All methods are implemented in the `deepgp` package on CRAN.

Keywords: surrogate, sparse matrix, nearest neighbor, uncertainty quantification, non-stationary

1 Introduction

Virtualization and simulation increasingly play a fundamental role in the design and study of complex systems that are either impossible or infeasible to experiment with directly. Examples abound in engineering (e.g., [Zhang et al., 2015](#)), aeronautics (e.g., [Mehta et al., 2014](#)), economics (e.g., [Kita et al., 2016](#)), and ecology (e.g., [Johnson, 2008](#)), to name a few. Simulation is “cheaper” than physical experimentation, but not “free”. Associated computational costs often necessitate statistical surrogates, meta-models that furnish accurate predictions and appropriate uncertainty quantification (UQ) from a limited simulation campaign. Surrogates may thus stand-in for novel simulation to support downstream tasks such as calibration ([Kennedy and O’Hagan, 2001](#)), optimization ([Jones et al., 1998](#)), and sensitivity analysis ([Marrel et al., 2009](#)). Surrogate accuracy, combined with effective UQ, is key to the success of such enterprises.

Gaussian processes (GPs) are a common surrogate modeling choice ([Rasmussen and Williams, 2005](#); [Gramacy, 2020](#)) because they offer both accuracy and UQ in a semi-analytic nonparametric framework. However, inference for GPs requires the evaluation of multivariate normal (MVN) likelihoods, which involves dense matrix decompositions that scale cubically with the size of the training data. Computer simulation campaigns used to be small, but recent advances in hardware, numerical libraries, and STEM training have democratized simulation and led to massively larger campaigns (e.g., [Marmin and Filippone, 2022](#); [Kaufman et al., 2011](#); [Lin et al., 2021](#); [Sun et al., 2019](#); [Liu and Guillas, 2017](#)). The literature has

*Corresponding author: Department of Statistics, Virginia Tech, anniees@vt.edu

[†]Department of Statistics, Virginia Tech

since adapted to this bottleneck by borrowing ideas from machine learning and geo-spatial GP approximation. Examples include sparse kernels (Melkumyan and Ramos, 2009), local approximations (Emery, 2009; Gramacy and Apley, 2015; Cole et al., 2021), inducing points (Quinonero-Candela and Rasmussen, 2005; Finley et al., 2009), and random feature expansions (Lázaro-Gredilla et al., 2010). See Heaton et al. (2019) and Liu et al. (2020a) for thorough reviews. Here we are drawn to a family of methods that leverage “Vecchia” approximation (Vecchia, 1988), which imposes a structure that generates a sparse Cholesky factorization of the precision matrix (Katzfuss et al., 2020a; Datta, 2021). When appropriately scaled or generalized (Stein et al., 2004; Stroud et al., 2017; Datta et al., 2016; Katzfuss and Guinness, 2021), and matched with sparse-matrix and multi-core computing facilities, Vecchia-GPs dominate competitors (Katzfuss et al., 2020b) on the frontier of accuracy, UQ, and speed.

Despite their prowess in many settings, GPs (and many of their approximations) are limited by the assumption of stationarity; they are not able to identify spatial changes in input–output regimes or abrupt shifts in dynamics. Here too, myriad remedies have been suggested across disparate literatures. Common themes include partitioning (e.g., Kim et al., 2005; Gramacy and Lee, 2008; Rushdi et al., 2017; Park and Apley, 2018), evolving kernels (Paciorek and Schervish, 2003; Picheny and Ginsbourger, 2013), and injective warpings (Zammit-Mangion et al., 2021). Deep Gaussian processes (DGPs) – originating in geo-spatial communities (Sampson and Guttorp, 1992; Schmidt and O’Hagan, 2003) but recently popularized by Damianou and Lawrence (2013) with analogy to deep neural networks – address this stationary limitation by layering GPs as functional compositions. Inputs are fed through intermediate Gaussian layers, which act as “warped” versions of the original inputs, before reaching the response. The structure of a DGP is equivalent to that of a “linked GP” (Ming and Guillas, 2021), except that middle layers remain unobserved. When the data generating mechanism is non-stationary, DGPs offer great promise. When regimes change abruptly, DGPs mimic partition schemes. When dynamics change more smoothly, they mimic kernel evolution. When stationary, they gracefully revert to ordinary GP dynamics via identity warpings.

Or at least that’s the sales pitch. In practice things are more murky because non-stationary flexibility is intimately twinned with training data size and structure. Unless the experiment can be designed to squarely target locations of regime change (Sauer et al., 2022), a large training data set is needed before these dynamics can be identified. Cubic scaling in flops is present in multitude, with large dense matrices at each latent DGP layer. Moreover, the unobserved/latent layers pose a challenge for statistical inference as they may not be analytically marginalized *a posteriori*. Markov chain Monte Carlo (MCMC) sampling (Sauer et al., 2022; Ming et al., 2021) exacerbates cubic bottlenecks and limits training data sizes to the hundreds. Approximate variational inference (VI) offers a thriftier alternative to full posterior integration (Damianou and Lawrence, 2013; Salimbeni and Deisenroth, 2017), but at the expense of UQ. VI for DGPs does not in-and-of-itself circumvent cubic expense, but, when coupled with inducing points and mini-batching (Ding et al., 2021), can be scaled up; allow us to defer a thorough review to Section 4. We find these approaches to be ill-suited to our computer surrogate modeling setting, in which signal-to-noise ratios are high and UQ is a must. We speculate this is because those libraries target benchmark machine learning examples for classification, or for regression settings with high noise.

In this work we expand the utility and reach of fully Bayesian posterior inference for DGP surrogate models through Vecchia approximation at each Gaussian layer. We explore strategic updating of the so-called “neighborhood sets” involved, based on the warpings of intermediate layers. With careful consideration of the myriad specifications in this hybrid context, we demonstrate that a Vecchia-DGP need not sacrifice predictive power nor UQ compared to a full (un-approximated) analog. We also show that it outperforms approximate DGP competitors in both accuracy and UQ on data sizes up to 100,000. An open-source implementation is provided in the `deepgp` package on CRAN (Sauer, 2022).

The remainder of the paper is organized as follows. Section 2 establishes notation while reviewing GPs,

DGPs, and Vecchia approximation. Section 3 details our Vecchia-DGP framework. Section 4 discusses implementation and reviews related work on/software for large scale DGP inference with an eye toward contrast and to set up benchmark exercises presented in Section 5. That section concludes with a study of a real-world satellite drag computer experiment. A brief discussion is offered in Section 6.

2 Review of major themes

2.1 Gaussian processes: shallow and deep

Let $f : \mathbb{R}^d \rightarrow \mathbb{R}$ represent a (possibly noisy) black-box function, say to abstract a computer model simulation. Consider inputs X of size $n \times d$ and corresponding outputs/observations $Y = f(X)$ of size $n \times 1$. Throughout we use lowercase x_i to refer to the i^{th} (transposed) row of X , and likewise for Y . Generic GP regression assumes a MVN over the response, $Y \sim \mathcal{N}_n(\mu(X), \Sigma(X))$. We specify $\mu(X) = 0$, as is common in surrogate modeling (Gramacy, 2020), yielding the likelihood

$$\mathcal{L}(Y | X) \propto |\Sigma(X)|^{-1/2} \exp\left(-\frac{1}{2}Y^\top \Sigma(X)^{-1}Y\right). \quad (1)$$

Above “ \propto ” indicates a dropped multiplicative constant. All of the action is in $\Sigma(X)$, which is usually specified pairwise as a function of Euclidean distance between rows of X :

$$\Sigma(X)^{ij} = \Sigma(x_i, x_j) = \tau^2 \left(k\left(\frac{\|x_i - x_j\|^2}{\theta}\right) + g\mathbb{I}_{i=j} \right). \quad (2)$$

Any choice of *kernel* $k(\cdot)$ leading to positive definite $\Sigma(X)$ is valid. Most often these are exponentially decreasing in their argument. Popular choices include the squared exponential and Matérn (Stein, 1999), but our work here is not kernel specific. Hyperparameters τ^2 , θ , and g govern the scale, lengthscale, and noise respectively, working together to describe signal-to-noise relationships.

There are many variations on this theme. For example, vectorized θ allow the rate of decay of correlation to vary with input direction. Such embellishments implement a form of *anisotropy*, a term preferred in geo-spatial contexts, or *automatic relevance determination* in machine learning (Liu et al., 2020b). We do not need such modifications in our DGP setup; once latent layers are involved, such flexibility manifests more parsimoniously via those values. Several of our competitors [Section 5] do utilize additional hyperparameters and/or equivalent affine pre-scaling (Wycoff et al., 2021).

Settings of (τ^2, θ, g) may be fitted through the likelihood (1), now viewing (X, Y) as training data. While derivative-based maximization is possible with numerical solvers, we prefer full posterior inference. We usually fix g at a small constant, e.g., $g = 10^{-6}$, as is appropriate for deterministic (or very low noise) computer model simulations. However, we don’t see this as a limitation of our contribution, and our software allows for this parameter to be inferred if needed. Further discussion is reserved for Section 6. Regardless of these choices, evaluation of the likelihood (1) relies on both the inverse and determinant of $\Sigma(X)$. For a dense $n \times n$ matrix, this is an $\mathcal{O}(n^3)$ operation with conventional libraries.

Conditioned on training data and covariance formulation $\Sigma(\cdot)$, predictions at testing locations \mathcal{X} (of size $n_p \times d$) follow Eq. (3) after extending $\Sigma(\mathcal{X}, X)$ to cover rows of \mathcal{X} paired with X following Eq. (2):

$$\mathcal{Y} | Y, X \sim \mathcal{N}_{n_p}(\mu', \Sigma') \quad \text{where } \mu' = \Sigma(\mathcal{X}, X)\Sigma(X)^{-1}Y \text{ and } \Sigma' = \Sigma(\mathcal{X}) - \Sigma(\mathcal{X}, X)\Sigma(X)^{-1}\Sigma(X, \mathcal{X}). \quad (3)$$

This closed-form is convenient but requires the inverse of $\Sigma(X)$, or at least a clever linear solve.

The above GP specification is *stationary* because only relative positions of training and testing inputs are involved (2). Consequently, identical input–output dynamics apply everywhere in the input space,

which can be limiting for some computer simulations. A great example comes from aeronautics/fluid dynamics. Lift forces on aircraft are fundamentally different at high speed versus low, and the transition at the sound barrier is abrupt (Pamadi et al., 2004). Several strategies to relax stationarity were introduced in Section 1. Here we consider deep Gaussian processes (DGP; Damianou and Lawrence, 2013) which nonlinearly warp inputs into a plausibly stationary regime. DGPs are functional compositions of GPs – the outputs of one GP feed as inputs to another. These intermediate Gaussian layers combine to bring some input locations closer together while spacing others further apart; a visual will be provided momentarily. While DGPs may extend several layers deep, we restrict our discussion here to two layers for simplicity. No part of our contribution (nor software) is strictly limited to this choice, although there is empirical evidence of diminishing returns for deeper DGP surrogates (Rajaram et al., 2021; Sauer et al., 2022).

A two-layer DGP with latent layer W is modeled as

$$Y | W \sim \mathcal{N}_n(0, \Sigma(W)), \quad W_k \stackrel{\text{ind}}{\sim} \mathcal{N}_n(0, \Sigma_k(X)), \quad k = 1, \dots, p. \quad (4)$$

$W = [W_1, \dots, W_p]$ is an $n \times p$ matrix with each row representing one observation and each column representing a dimension of the latent space. We adopt the deep learning convention of referring to the component dimensions of W as “nodes”. Each node has its own $\Sigma_k(X)$ which may or may not share features, like kernels and hyperparameters, with others. In our setting we specify unit scale and zero noise on latent layers (i.e., $\tau^2 = 1$ and $g = 0$ within $\Sigma_k(X)$) in order to preserve parsimony and identifiability. It is common to fix $p = d$, but autoencoding setups which “squeeze through” lower-dimensional latent layers ($p \ll d$) are not uncommon in high-dimensional settings (Domingues et al., 2018). Again, our work and implementation are not limited to this choice.

Inference for DGPs, including for hyperparameters buried in the Σ s, requires integration over W :

$$\mathcal{L}(Y | X) = \int \mathcal{L}(Y | W) \prod_{k=1}^p \mathcal{L}(W_k | X) dW, \quad (5)$$

with $\mathcal{L}(Y | W)$ and $\mathcal{L}(W_k | X)$ following Eq. (1), or slight variations thereupon. However, this integral is not analytically tractable. The prevailing inferential tools thus rely either on approximate variational methods (Damianou and Lawrence, 2013; Salimbeni and Deisenroth, 2017) or sampling (Dunlop et al., 2018; Havasi et al., 2018; Ming et al., 2021).

Our preferred inferential scheme, detailed in Sauer et al. (2022), prioritizes UQ through a fully-Bayesian MCMC algorithm, hinging on elliptical slice sampling (ESS; Murray et al., 2010) of latent layers. ESS is specifically designed for sampling variables with MVN priors, is notably free of tuning parameters, and works well in DGP settings (also see Ming et al., 2021). We further embrace a Bayesian treatment of kernel hyperparameters: marginalizing τ^2 from the posterior under a reference prior (Gramacy, 2020, Chapter 5) and adopting Metropolis-Hastings (MH; Hastings, 1970) sampling of θ ’s (each $\Sigma(W)$ and $\Sigma_k(X)$ with unique lengthscale), all wrapped in a Gibbs scheme. This approach is thorough but computationally demanding. Each Gibbs iteration requires many evaluations of Gaussian likelihoods (1), and several thousands of iterations are needed to burn-in and then explore the posterior.

As an example of DGP warping, consider the two-dimensional “G-function”, featured later in Section 5.1. A visual is provided in the left panel of Figure 1. This function is characterized by inclines and abrupt shifts. A stationary “shallow” GP is unable to distinguish between the steep sloping regions in the corners and the valley regions that form a cross shape in the center. Figure 1 also shows a posterior sample (i.e., a burned-in ESS draw) of the hidden layer W plotted two ways. The middle panels show each of two “nodes” as a function of X . Each node is a conditionally independent stationary GP. These nodes depart from the identity mapping (i.e. $W_1 = X_1$ and $W_2 = X_2$) by stretching the inputs along the

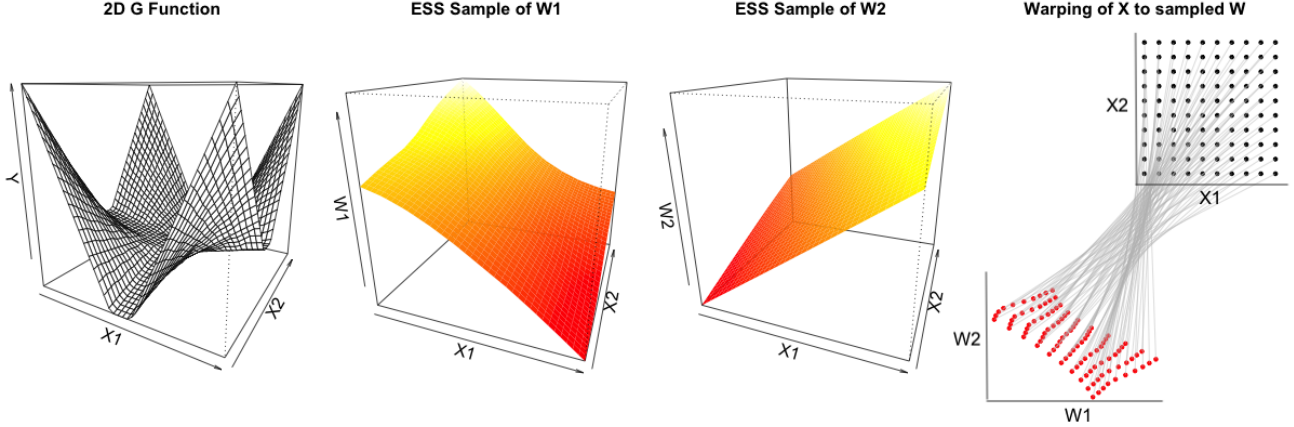


Figure 1: (Left) Visual of the 2d G-function. (Middle Left/Middle Right) Posterior sample of W for a two-layer DGP fit to the data of the left panel, comprised of two “nodes” (one in each panel). (Right) The resulting “warping” of this sample as evenly gridded X are mapped to W .

diagonal. The right panel shows the combined “warping” effect that both nodes have on the evenly gridded X . Since only pair-wise distances feed into the final layer (through $\Sigma(W)$), the warping effect is invariant to rotations and translations. ESS samples of W that “bounce” between mirror images of themselves are taken as an indication that the chain is mixing well. In Section 5.1 we show that the warping(s) in the figure accommodate the G-function’s non-stationary dynamics better than many other methods.

2.2 Vecchia approximation

The Vecchia approximation (Vecchia, 1988) is motivated by computational bottlenecks in GP regression, which are compounded in a DGP setting. The underlying idea is basic: any joint distribution can be factored into a product of conditionals $p(y) = p(y_1)p(y_2 | y_1)p(y_3 | y_2, y_1) \cdots p(y_n | y_{n-1}, \dots, y_1)$. This is true up to any re-indexing of the y_i ’s. In particular, and to establish some notation for later, any joint likelihood (1) may be factored into a product of univariate likelihoods

$$\mathcal{L}(Y) = \prod_{i=1}^n \mathcal{L}(y_i | Y_{c(i)}) \quad (6)$$

where $c(1) = \emptyset$ and $c(i) = \{1, 2, \dots, i-1\}$ for $i = 2, \dots, n$. The Vecchia approximation instead takes a subset, $c(i) \subset \{1, 2, \dots, i-1\}$, of size $|c(i)| = \min(m, i-1)$. When $m < n$, the strict equality of Eq. (6) is technically an approximation, yet we will use equality notation throughout when speaking of the general case with unspecified m . This approximation is indexing-dependent for fixed $m < n$, but hold that thought for a moment. Crucially Eq. (6), in the context of Eqs. (1) and (3), induces a sparse precision matrix: $Q(X) = \Sigma(X)^{-1}$. The (i, j) th element of $Q(X)$ is 0 if and only if y_i and y_j are conditionally independent (i.e. $i \notin c(j)$ and $j \notin c(i)$). The Cholesky decomposition of the precision matrix, U_x for $Q(X) = U_x U_x^\top$, is even sparser with fewer than m off-diagonal non-zero entries in each row. We follow Katzfuss et al. (2020a) in working with the upper triangular U_x , referred to as the “upper-lower” Cholesky decomposition.

A GP-Vecchia approximation requires two choices: an ordering of the data and selection of conditioning sets $c(i)$. There are many orderings that work well (Stein et al., 2004; Guinness, 2018; Katzfuss and Guinness, 2021), but a simple random ordering is common (Stroud et al., 2017; Datta et al., 2016; Wu et al., 2022). The prevailing choice for conditioning sets is “nearest-neighbors” (NN) in which $c(i)$ comprises of integers indexing the closest observations to x_i which appear earlier in the ordering. Approximations

based on NN are sometimes referred to as NN-GPs (Datta et al., 2016). To demonstrate an ordering and NN conditioning set, the left panel of Figure 2 shows a grid of inputs with random ordering (the numbers plotted). [The other panels will be discussed in Section 3.] For point $i = 45$ (triangle), the NN conditioning set of size $m = 10$ is highlighted by circles. These are the points closest to x_{45} in Euclidean distance, with indices $j < i$ in the ordering. Sets $c(i)$ for all $i = 1, \dots, 100$ are chosen similarly.

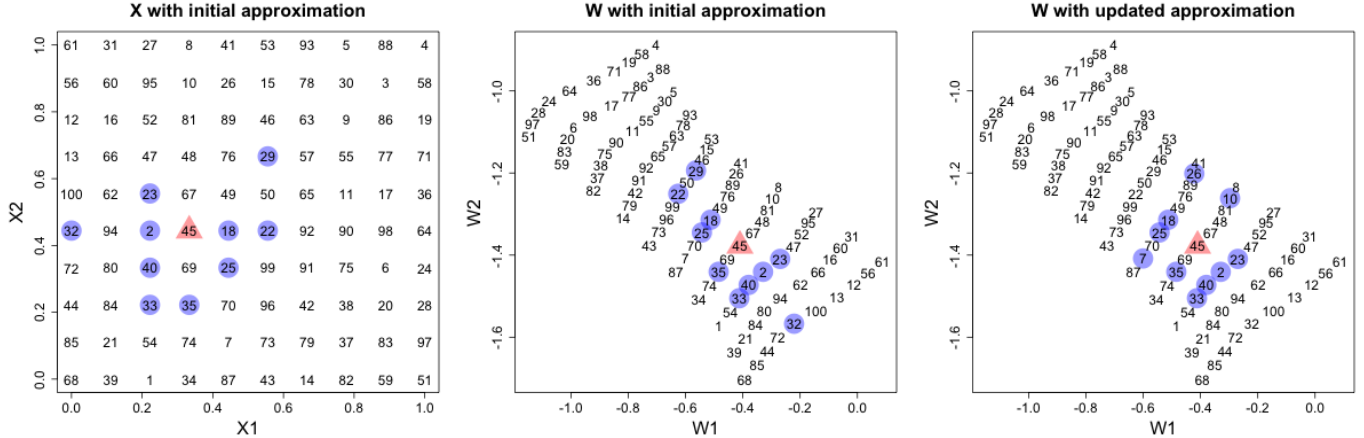


Figure 2: (Left) A uniformly spaced grid of inputs, randomly ordered. NN conditioning set for x_{45} (triangle) is highlighted by circles. (Middle) Same ordering/NN sets instead plotted as the “warped” W from Figure 1. (Right) “Warped” W with NN conditioning adjusted accordingly.

Under a GP, components of Eq. (6) are univariate Gaussian, $\mathcal{L}(y_i | Y_{c(i)}) \sim \mathcal{N}_1(\mu_i(X), \sigma_i^2(X))$, where

$$B_i(X) = \Sigma(x_i, X_{c(i)})\Sigma(X_{c(i)})^{-1}, \quad \mu_i(X) = B_i(X)Y_{c(i)}, \quad \sigma_i^2(X) = \Sigma(x_i) - B_i(X)\Sigma(X_{c(i)}, x_i) \quad (7)$$

and $X_{c(i)}$ is the row-combined matrix of X ’s rows corresponding to indices $c(i)$. Foreshadowing a DGP application in Section 3, one may define $B_i(W)$, $\mu_i(W)$ and $\sigma_i^2(W)$ identically but with w/W in place of x/X . With this representation, we convert a large $n \times n$ matrix inversion ($\mathcal{O}(n^3)$) into n -many $m \times m$ matrix inversions ($\mathcal{O}(nm^3)$), a significant improvement if $m \ll n$.

The details of Vecchia-GPs, including numerous options for orderings, conditioning sets, hyperparameterizations, and computational considerations, are spread across multiple works (e.g., Katzfuss et al., 2020a; Katzfuss and Guinness, 2021; Guinness, 2018, 2021; Datta et al., 2016; Datta, 2021; Finley et al., 2019). These specifications, along with software implementations (e.g. Katzfuss et al., 2020c; Guinness et al., 2021; Finley et al., 2020), can be rather complex. We do not need such hefty machinery in our DGP setup for computer surrogate models. Much of our research effort involved sifting through this literature to determine what is essential and which variations work best for DGP surrogates. As one example, latent layers W and deterministic $Y = f(\cdot)$ utilize noise free modeling (small/zero nugget g), which affords several simplifications. In particular, we do not follow Datta et al. (2016) and Katzfuss and Guinness (2021) in distinguishing between noisy observations and latent “true” variables. This greatly streamlines development [Section 3] and reduces computational demands.

3 Vecchia-approximated deep Gaussian processes

Here we detail our Vecchia-DGP model, posterior integration, and other implementation considerations. Our focus remains on two-layer models for simplicity; extension to deeper DGPs comes down to iteration.

We begin by fixing ordering and conditioning; ideas to tailor these to the DGP context follow later in Section 3.3. Our software implementation [Section 4.1], supports a wider array of options than those enumerated here, including deeper (Vecchia) DGPs and estimating nuggets for smoothing noisy data [Section 6].

3.1 Inferential building blocks

We impose the Vecchia approximation at each layer of the DGP. Leveraging sparsity of the upper-lower Cholesky decomposition of the precision matrices, a two-layer Vecchia-DGP model may be represented as

$$Y | W \sim \mathcal{N}_n \left(0, (U_w U_w^\top)^{-1} \right) \quad W_k \stackrel{\text{ind}}{\sim} \mathcal{N}_n \left(0, \left((U_x^{(k)})(U_x^{(k)})^\top \right)^{-1} \right), \quad k = 1, \dots, p, \quad (8)$$

where $\Sigma(W)^{-1} = U_w U_w^\top$ and $\Sigma_k(X)^{-1} = (U_x^{(k)})(U_x^{(k)})^\top$. Each W_k , having its own Gaussian prior, *also* has its own Vecchia decomposition. Often these $U_x^{(k)}$ will share conditioning sets but have disparate hyperparameterization, e.g., unique lengthscales $\theta_x^{(k)}$. When $m = n$, this formulation is equivalent to Eq. (4). When $m < n$, U_w and $U_x^{(k)}$ have induced sparsity.

We aim to conduct full posterior integration for this model, extending Eq. (5) to include integration over hyperparameters, but, as in Section 2.1, this is not analytically tractable. Posterior sampling via ESS and MH regarding $\mathcal{L}(Y | W)$ and $\mathcal{L}(W_k | X)$ requires three ingredients: (i) prior sampling, (ii) likelihood evaluation, and (iii) prediction at unobserved inputs. These are detailed here, for the model in Eq. (8), in turn. We shall focus on $\mathcal{L}(Y | W)$, but the idea is immediately extendable to $\mathcal{L}(W_k | X)$. Both are GPs, so the details only differ superficially in notation, and with iteration over $k = 1, \dots, p$. Ultimately, these “building blocks” tie together to support posterior sampling, with details following in Section 3.2.

(i) Prior. Direct sampling of $Y^\star \sim \mathcal{N}_n(0, (U_w U_w^\top)^{-1})$, often called “conditional simulation”, involves individually drawing $y_i^\star \sim \mathcal{N}_1(B_i(W)Y_{c(i)}^\star, \sigma_i^2(W))$ for $B_i(W)$ and $\sigma_i^2(W)$ defined with analogy to Eq. (7). An important difference, however, is that the application here crucially relies on *previously sampled* $Y_{c(i)}^\star$, meaning each y_i^\star must be sampled *sequentially*. With an eye towards parallel implementation [Section 4.1], we instead leverage the sparsity of the upper-triangular U_w . [Katzfuss and Guinness \(2021, Proposition 1\)](#) derived a closed-form solution for populating U_w , with $(j, i)^{\text{th}}$ entry

$$U_w^{ji} = \begin{cases} \frac{1}{\sigma_i(W)} & i = j \\ -\frac{1}{\sigma_i(W)} B_i(W) [\text{index of } j \in c(i)] & j \in c(i) \\ 0 & \text{otherwise} \end{cases} \quad (9)$$

for $B_i(W)$ and $\sigma_i(W)$ in Eq. (7). With U_w in hand, sampling Y^\star follows [Gelman et al. \(2013, App. A\)](#):

$$Y^\star = (U_w^\top)^{-1} z \quad \text{where } z \sim \mathcal{N}_n(0, \mathbb{I}). \quad (10)$$

Strategically, we avoid matrix inversions by using a forward solve of $U_w^\top Y^\star = z$.

(ii) Likelihood. Evaluations of $\mathcal{L}(Y | W)$ could similarly be calculated as the product of univariate Gaussian densities, combining Eqs. (6–7) via $\mathcal{L}(y_i | W) \sim \mathcal{N}_1(\mu_i(W), \sigma_i^2(W))$. We instead choose to leverage the sparse U_w formulation (9), yielding the log likelihood

$$\begin{aligned} \log \mathcal{L}(Y | W) &\propto \log |(U_w U_w^\top)^{-1}|^{-1/2} - \frac{1}{2} Y^\top U_w U_w^\top Y \\ &\propto \sum_{i=1}^n \log(U_w^{ii}) - \frac{1}{2} Y^\top U_w U_w^\top Y, \end{aligned} \quad (11)$$

in which the sparse structure of U_w allows for thrifty matrix multiplications.

(iii) Prediction. Given observed $Y \mid W \sim \mathcal{N}_n(0, (U_w U_w^\top)^{-1})$, i.e., training observations Y and a burned-in ESS sample of W , we wish to predict \mathcal{Y} for an $n_p \times d$ matrix of novel \mathcal{W} . Note these novel \mathcal{W} ultimately arise as samples following analogous application of the very same procedure we are about to describe, except for W_k as the “response” drawn at novel testing sites \mathcal{X} (more on this in Section 3.2). The simplest approach treats each row of \mathcal{W} independently. Independent prediction is sufficient if only point-wise means and variances are required, as is common in many downstream surrogate modeling tasks. For each $i = 1, \dots, n_p$, we form $c(i)$ with m training locations from W (details in Section 3.3). This imposes conditional independence among \mathcal{Y}_i (i.e., \mathcal{Y}_i is not conditioned on \mathcal{Y}_j for $i \neq j$). The posterior predictive distribution then follows $\mathcal{Y}_i \sim \mathcal{N}_1(\mu_i(W), \sigma_i^2(W))$ with $\mu_i(W)$ and $\sigma_i^2(W)$ defined as in Eq. (7).

This independent treatment is fast and easily parallelized over index $i = 1, \dots, n_p$. Consequently, it is the method we prefer for the benchmarking exercises of Section 5, involving a cumbersome additional layer of Monte Carlo (MC) over training–testing partitions. Yet an imposition of independence among \mathcal{Y} can be limiting. In some cases, joint prediction utilizing the full covariance structure $\mathcal{Y} \mid Y, W \sim \mathcal{N}_{n_p}(\mu^*, \Sigma^*)$ is essential. We can accommodate such settings as follows. First append \mathcal{W} indices to the existing ordering of W , ensuring predictive locations are ordered *after* training locations, forming the full ordering $i = 1, \dots, n, n + 1, \dots, n + n_p$. Conditioning sets $c(i)$ for $i = n + 1, \dots, n + n_p$ index *any* observations from W or \mathcal{W} with indices prior to i in the combined ordering, thus allowing predictive outputs to potentially condition on other predictive outputs, in addition to nearby training data observations.

Next, “stack” training and testing responses in the usual way (Gramacy, 2020, Section 5.1.1)

$$\begin{bmatrix} Y \\ \mathcal{Y} \end{bmatrix} \sim \mathcal{N}_{n+n_p}(0, \Sigma_{\text{stack}}) \quad \text{where} \quad \Sigma_{\text{stack}} = \Sigma \left(\begin{bmatrix} W \\ \mathcal{W} \end{bmatrix} \right) = \begin{bmatrix} \Sigma(W) & \Sigma(W, \mathcal{W}) \\ \Sigma(\mathcal{W}, W) & \Sigma(\mathcal{W}) \end{bmatrix}.$$

Then leverage (9) to analogously populate a “stacked” upper-lower Cholesky decomposition,

$$U_{\text{stack}} = \begin{bmatrix} U_w & U_{w, \mathcal{W}} \\ 0 & U_{\mathcal{W}} \end{bmatrix} \quad \text{such that} \quad \Sigma_{\text{stack}} = \left(U_{\text{stack}} U_{\text{stack}}^\top \right)^{-1} = \left(\begin{bmatrix} U_w U_w^\top + U_{w, \mathcal{W}} U_{w, \mathcal{W}}^\top & U_{w, \mathcal{W}} U_{\mathcal{W}}^\top \\ U_{\mathcal{W}} U_{w, \mathcal{W}}^\top & U_{\mathcal{W}} U_{\mathcal{W}}^\top \end{bmatrix} \right)^{-1}.$$

An application of the partition matrix inverse identities (details in App. C.1–C.2) results in the following posterior predictive moments, after applying the usual MVN conditioning identities for $\mathcal{Y} \mid Y, W$ (3):

$$\mathcal{Y} \mid Y, W \sim \mathcal{N}_{n_p}(\mu^*, \Sigma^*) \quad \text{for} \quad \mu^* = -(U_{\mathcal{W}}^\top)^{-1} U_{w, \mathcal{W}}^\top Y \quad \text{and} \quad \Sigma^* = \left(U_{\mathcal{W}} U_{\mathcal{W}}^\top \right)^{-1}. \quad (12)$$

These are simplified versions of the moments provided by Katzfuss et al. (2020a), thanks to a streamlined latent structure and the imposition that predictive locations must be ordered after training locations. Naturally, if no predictive locations condition on others then $U_{\mathcal{W}}$ and Σ^* will be diagonal, and we can return to the simpler implementation of independent predictions.

Katzfuss et al. (2020a) remark that conditioning on other predictive locations, i.e., using joint μ^* and Σ^* , is more accurate than conditioning only on training data. Anecdotally, in our own empirical work, we have found this difference to be inconsequential. Unless a joint Σ^* is required, say for calibration (Kennedy and O’Hagan, 2001), we prefer the faster, parallelizable, independent approach. (Both are provided by our software; more in Section 4.1.) In settings where it might be desirable to reveal/leverage posterior predictive correlation, but perhaps it is too computationally burdensome to work with n_p^2 pairs of testing sites simultaneously, a hybrid or batched scheme might be preferred.

3.2 Posterior inference

Building blocks (i–iii) in hand, posterior sampling by MCMC may commence following Algorithm 1 of Sauer et al. (2022). In other words, the underlying inferential framework is unchanged modulo an efficient (Vecchia) method for (i) prior sampling, (2) likelihood evaluation, and (3) prediction. Rather than duplicate details here, allow us point out a few relevant highlights. In model training, every evaluation of a Gaussian likelihood utilizes Eq. (11), whether for inner (W_k) or outer (Y), matched with $U_x^{(k)}$ and U_w , respectively, and with appropriate covariance hyperparameters, e.g., $\theta_x^{(k)}$, embedded into the $B_i(\cdot)$ and $\sigma_i(\cdot)$ components of said U matrices (9). When employing ESS for $W^{(k)}$, say, random samples from the prior follow Eq. (10). The MCMC scheme remains unchanged modulo Vecchia approximation everywhere under-the-hood.

To predict at unobserved inputs \mathcal{X} , i.e., Section 4.1 of Sauer et al. (2022), replace traditional GP prediction at each Gaussian layer (3) with its Vecchia counterpart (12). For each candidate (burned-in/thinned) MCMC iteration, predictive locations \mathcal{X} are mapped to “warped” locations \mathcal{W} , which are then mapped to posterior moments for \mathcal{Y} , with each step following Eq. (12). The resulting moments are post-processed, with ergodic averages yielding the final posterior predictive moments. Sauer et al. (2022) focused on small training and testing sets, so their setup favored samples from a joint predictive distribution analogous to Eq. (12). These may be replaced with independent point-wise, and parallelized predictions as described in Section 3.1 in the presense of a large/dense testing set. We remind the reader that a DGP predictive distribution is not strictly Gaussian, even though it arises as an integral over Gaussians. However we find that ergodic averages, represented abstractly here by empirical moments $\bar{\mu}$ and $\bar{\Sigma} + \text{Cov}(\mu)$ through the law of total variance, are a sufficient substitute for retaining thousands of high-dimensional MCMC draws of μ^* and Σ^* , say, or their pointwise analogues.

It is important to briefly acknowledge the substantial computation inherent in this inferential scheme. The requisite MCMC requires thousands of iterations, each of which necessitates multiple likelihood (11) evaluations. Predictions require averaging across these draws, although thinning can reduce this effort. Despite these hefty computational demands, efficient parallelization (described in more detail momentarily), strategic initializations of latent layers, and other sensible pre-processing yield feasible compute times even with large data sizes. For example, the Vecchia-DGPs of Section 5.2 with $n = 100,000$ were fit in 26 hours on a 16-core machine. We aim to show that this investment pays dividends compared to faster GP and DGP alternatives in terms of prediction accuracy and UQ [Section 5].

3.3 Ordering and conditioning

Each Gaussian component of the DGP could have its own ordering and conditioning set, $c_x^{(k)}(i)$ for $U_x^{(k)}$ and $c_w(i)$ for U_w in the two-layer model, in which orderings denoted by i need not be the same. Since each $c_x^{(k)}(i)$ acts on the same input space, we simplify the approximation by sharing ordering and conditioning sets across $k = 1, \dots, p$, resulting in only two orderings and two conditioning sets, $c_x(i)$ and $c_w(j)$.

These choices are not part of the stochastic process describing the data generating mechanism, although that is an interesting possibility we discuss in Section 6. A consequence of this is that once a chain has been initialized under a particular ordering, yielding U_x or U_w up to hyperparameters like θ which are included in the hierarchy describing the stochastic process, $c_x(i)$ and $c_w(j)$ must remain fixed throughout the MCMC in order to maintain detailed balance. It occurred to us to try randomizing over orderings from one MCMC iteration to the next, but the chain does not burn in/achieve stationarity. Each change to one of $c_x(i)$ or $c_w(j)$ causes the chain to “jump” somewhere else. Nevertheless, it could be advantageous to customize aspects of a Vecchia ordering and conditioning dynamically, say based on a DGP fit or other analysis, or to hedge by averaging results from multiple orderings. This is fine with independent chains.

With this in mind, we adopt the following setup. Begin with a random ordering of indices for each DGP layer. This follows the recommendation of Guinness (2018) and mirrors other recent work on NNGPs (Wu et al., 2022; Datta et al., 2016; Stroud et al., 2017). Then select conditioning sets based on NN, as eponymous in the NNGP/Vecchia literature. In X -space, calculating $c_x(i)$ as the $\min(m, i - 1)$ nearest points (of lower index) is straightforward. These locations are anchored in place by the experimental design. For latent Gaussian layer W , NN conditioning sets can be more involved. Since W is unobserved, we start with no working knowledge of the nature of the warping. (Our prior is mean-zero Gaussian under a distance-based covariance structure with unknown hyperparameterization.) A good automatic initialization for the MCMC is to assume no warping (i.e. $W = X$). In that setting, NN for W based on relative Euclidean distance in X space is sensible.

Such a conditioning set is even workable after considerable posterior sampling, whereby W may have diverged from the identity mapping with X . We find that in practice each individual nodes’ (i.e., W_k) contribution to the overall multidimensional warping for $k = 1, \dots, p$ is usually convex. As a visual, consider again Figure 2. The right two panels show conditioning sets (both NN in a certain sense) for W arising as a function of X corresponding to the mapping in Figure 1. The locations of the observations (marked by numbers) represent a warping of the original evenly-gridded inputs (left panel). The middle panel shows the conditioning set $c_w(45)$ that was selected based on NN in X space. Observe that these highlighted points are equivalent to those of the left panel.

Selecting $c_w(j)$ based on X is a good starting point, but we envision scope to be more strategic. Given posterior information about W , one may wish to update $c_w(j)$ in light of that warping. For example, NN on W could be calculated after burn-in and used as the basis of U_w conditioning for a re-started chain. Such an operation could be viewed as a nonlinear extension of sensitivity pre-warping Wycoff et al. (2021), tailored to the Vecchia approximation. The right panel of Figure 2 shows such a re-conditioning. There is some precedence for evolving neighborhood sets in this way from the ordinary Vecchia-GP literature. For example, Katzfuss et al. (2020b) use estimated multiple-lengthscale parameters to find NN based on re-scaled inputs $X/\sqrt{\theta}$, vectorizing over columns; Kang and Katzfuss (2021) extend that to full kernel/correlation based re-scaling. Both are situated in an optimization based inferential apparatus, and the authors describe a careful “epoch-oriented” scheme to circumvent convergence issues, analogous to maintaining detailed balance in MCMC. Our particular re-burn-in instantiation of this idea, described above, represents a natural extension: an affine warping of inputs for NN calculations is upgraded to a nonlinear one via latent Gaussian layers. Yet in our empirical work exploring this idea [Section 5.1], we disappointingly find little additional value realized by the extra effort for DGPs. We speculate in Section 6 that this may be because we haven’t yet encountered any applications demanding highly non-convex W .

A final consideration involves extending orderings and neighborhood sets to testing sites when sampling from the posterior predictive distribution. Here, we again use NN sets to select $c_x(i)$ and $c_w(j)$ for predictive/testing locations \mathcal{X} (which are mapped to \mathcal{W}). In X space, NN sets are fixed once for each row of \mathcal{X} . In W space, after MCMC sampling (i.e., model “training”), we leverage the learned warpings ($W^{(t)}$ for $t \in \mathcal{T}$) and calculate NNs in that space to maximize the efficacy of the approximation at each location: for each row of \mathcal{W} we re-calculate “warped” NN sets for each sample $W^{(t)}$. Resulting predictions are combined with expectation taken over all $t \in \mathcal{T}$. This re-calculation of $c_w(i)$ for each t requires extra effort, but it is not onerous and focuses computation where it is most needed.

4 Implementation and competition

Here we detail our implementation and provide evidence of substantial speedup compared to a full DGP utilizing the same underlying method but without a Vecchia approximation (Sauer et al., 2022). We see

this compartmentalization – identical computation modulo sparsity of inverse Cholesky factors – as one of the great advantages of our approach. To explain and contrast, we then transition to a discussion of other DGP variations where we find that engineering choices (for computational efficiency) are far more strongly coupled to modeling ones (for statistical fidelity), which can adversely affect performance in surrogate modeling settings, i.e., high-signal/low noise prediction with appropriate UQ.

4.1 Implementation

We provide an open-source implementation as an update to the `deepgp` package (Sauer, 2022) for R on CRAN. Although we embrace a bare-bones approach, our R/C++ implementations of the “building blocks” in Section 3.1 are heavily inspired by the more extensive `GPvecchia` (Katzfuss et al., 2020c) and `GpGp` (Guinness et al., 2021) packages. Computational speed relies on strategic parallelization and careful consideration of sparse matrices. For example, we utilize `OpenMP` pragmas to parallelize the calculation of each row of the sparse U_w and $U_x^{(k)}$ (9). We use `RcppArmadillo` (Eddelbuettel and Sanderson, 2014) in C++ and `Matrix` (Bates and Maechler, 2021) in R to handle sparse matrix calculations, aspects of which are also parallelized (but usually to a lesser degree) under-the-hood.

While our `Vecchia-DGP` implementation in `deepgp` is distinct from its full (un-approximated) counterpart, they share an interface for ease of use. A `vecchia` indicator to the existing `fit` functions triggers approximate inference, i.e.

```
R> fit <- fit_two_layer(x, y, vecchia = TRUE, m = 25, true_g = eps)
R> fit <- predict(fit, x_pred, lite = TRUE, m = 25)
```

The neighborhood size is specified as $m = m = \min\{25, n - 1\}$ by default, where choosing $n - 1$ results in no approximation, but still uses the `Vecchia` implementation, which is useful for debugging and benchmarking. Notice that training and prediction accommodate distinct m . We have found that $m = 25$ (for both) works well for our exercises here [further investigation in Supp. D], but it may be advantageous to use larger m for prediction or to scale m with n . We additionally allow `predict` calls to toggle between independent (`lite = TRUE`) or joint predictions (`lite = FALSE`).

A two-phase MCMC option, updating orderings and NN conditioning sets based on a burned-in warping [Section 3.3] is supported by `re_approx = TRUE` to `continue`, an S3 method automating additional MCMC from the end of a previous chain. The `true_g` argument is optional. If it is not provided, then a nugget is estimated along with other hyperparameters. In our experiments later we fix `eps = 1e-8` for all but the satellite drag example [Section 5.2] where we follow others in using `eps = 1e-4`.

To demonstrate computational improvements over the full un-approximated implementation, the left panel of Figure 3 compares the computation time of 1000 such MCMC iterations between the full implementation of Sauer et al. (2022) and our proposed `Vecchia-DGP`. A 16-core, hyperthreaded, Intel i9 CPU at 3.6GHz, was used to collect these timings. The full, non-`Vecchia` implementation experiences cubic-in- n costs and is not generally feasible for sample sizes above several hundred. The `Vecchia` implementation scales linearly-in- n , allowing for much larger data sizes. To contrast approaches to prediction outlined in Section 3.1, the right panel of Figure 3 shows computation times for `Vecchia-DGPs` on larger training data sizes with both independent (diamonds) and joint (stars) schemes. Observe that independent predictions scale linearly in both n and n_p , but joint predictions are more costly. Note the change in scale of the y -axes from the left to the right panel.

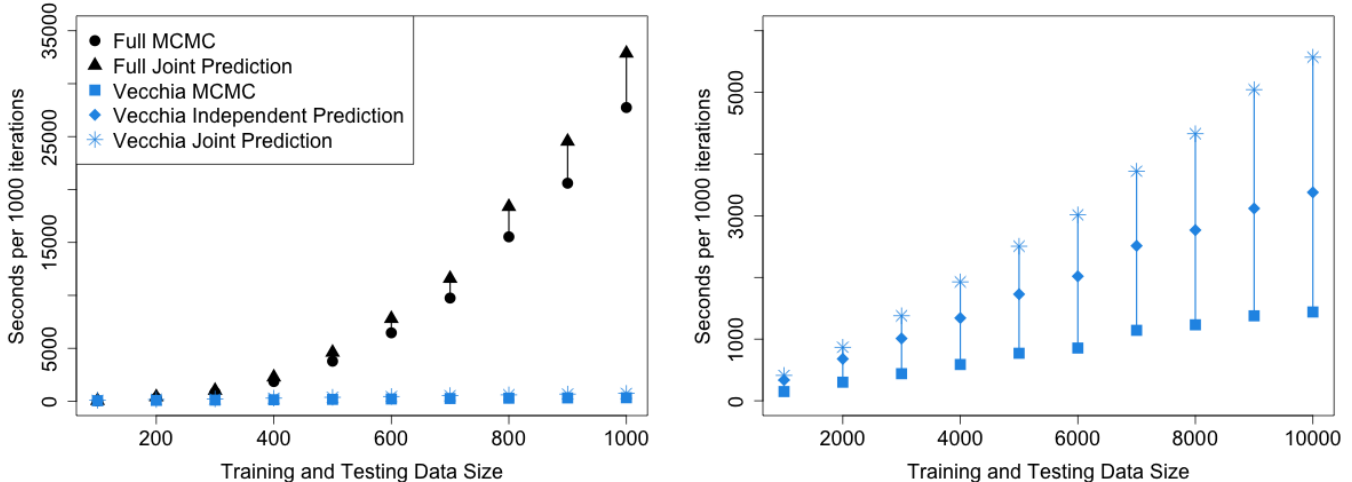


Figure 3: Computation time in seconds per 1000 MCMC iterations for a two-layer DGP fit to the 2d Schaffer function. Cumulative training and prediction times are connected by vertical lines. Times are reported for a full un-approximated DGP (smaller data sizes) and a Vecchia-approximated DGP ($m = 25$).

4.2 Competing methodology and software

As an alternative to MCMC, others have embraced variational inference (VI) in which the intractable DGP posterior (5) is approximated with a simpler family of distributions, often also Gaussian (Damianou and Lawrence, 2013). Inspired by deep neural networks, Bui et al. (2016) proposed an Expectation Propagation (EP) scheme for DGPs, which is closely related to VI. Salimbeni and Deisenroth (2017) broadened previous VI-like approaches for DGPs by allowing intra-layer dependencies, naming their method “doubly stochastic variational inference” (DSVI). These approaches optimize rather than integrate, which requires less work. However, optimization ignores uncertainty; the fidelity of a VI approximation is linked to the choice of variational family, rather than directly to computational effort. More MCMC always improves posterior resolution; more VI does not. Hyperparameters don’t neatly fit into variational families otherwise preferred for latent nodes, so they often get ignored, or their tuning is left to external validation schemes. By contrast, extra Metropolis easily accommodates a few more hyperparameters without hassle.

In order to handle training data sizes (n) upwards of hundreds of thousands, VI-based DGPs utilize *inducing points*, an umbrella term covering ideas developed separately as *pseudo-inputs* in machine learning (e.g., Snelson and Ghahramani, 2006) and as *predictive processes* in geostatistics (e.g., Banerjee et al., 2008). Inducing points impose a low-rank kernel structure by measuring distance-based correlations through a smaller subset of $m \ll n$ reference locations or “knots” in d -dimensions. Woodbury matrix identities improve decomposition of the implied full $n \times n$ structure from $\mathcal{O}(n^3)$ to $\mathcal{O}(nm^2)$. Although often framed as an “approximation”, inducing points can represent a fundamental change to the underlying kernel structure. Large n and m small enough to sufficiently speed up calculations can result in low-fidelity or “blurry” GP approximations (Wu et al., 2022). Moreover, optimizing inducing point placement can be fraught with challenges (e.g., Garton et al., 2020). DSVI uses k -means to place inducing points near clusters of inputs, but computer experiments often deploy space-filling designs which would ensure there are no clusters.

The Vecchia approximation offers an alternative to inducing points without introducing auxiliary quantities. Although it is sometimes cast as a novel modeling framework rather than an approximation (Datta et al., 2016), a key advantage is that it doesn’t fundamentally change the underlying kernel structure – at least not in the way inducing points do. Rather, it more subtly imposes sparsity in its inverse Cholesky

factor. Although Vecchia can be higher on the computational ladder ($\mathcal{O}(nm^3)$), it is able to provide good approximations with m much smaller than that required of inducing points without the “blur” or hassle in tuning the locations of $m \times d$ quantities. Wu et al. (2022) entertain Vecchia in lieu of inducing points for ordinary GPs via VI with favorable results. It may only be a matter of time before Vecchia is deployed with VI for DGPs. We prefer MCMC for its UQ properties.

Other alternatives to inducing points in a VI context have been suggested, including random feature expansion (RFE; Lázaro-Gredilla et al., 2010). Extending RFE from ordinary to DGPs has been the subject of several recent papers (Cutajar et al., 2017; Laradji et al., 2019; Marmin and Filippone, 2022), with some success. Others have taken the opposite route, keeping inducing points but swapping out VI for Hamiltonian Monte Carlo (HMC; Betancourt, 2017) for DGPs (Havasi et al., 2018). HMC has an advantage over VI in that hyperparameters can easily be subsumed into the inferential apparatus without external validation. We show [Section 5] that this leads to performance gains on predictive accuracy in surrogate modeling settings. Nevertheless, DSVI is generally considered the state-of-the-art for DGPs in machine learning. We think this is largely to do with computation and prowess in classification tasks. DSVI’s inducing point approximation enables mini-batching to massively distribute a stochastic gradient descent. This seems to work well in classification settings where resolution drawbacks are less acute, but our experience [Section 5] suggests this may not extend to the low-noise regression settings encountered in surrogate modeling of computer simulations.

Ultimately, benchmarking against such alternatives comes down to software, as even the best methodological ideas are only as good, in practice, as their implementations. DSVI is neatly packaged in `gpflux` for Python (Dutordoir et al., 2021), but requires specifying hyperparameters. Default settings were not ideal for our test problems, and we found manual tuning to be cumbersome. The sampling-based HMC implementation is available on the authors’ GitHub page (Havasi et al., 2018). This performs better, we think precisely because of its ability to more automatically tune hyperparameters in an Empirical Bayes/EM fashion, but uncertainty in these is not included in the posterior predictions. RFE software is on the authors’ GitHub page (Cutajar et al., 2017), but relies on the specification of myriad inputs, with few defaults provided. Despite attempts to port example uses to our surrogate modeling setting, we had limited success. We found that results were uniformly inferior to DSVI, and no predictive uncertainties were provided leading us to ultimately drop RFE from further consideration. Finally, EP is available on the authors’ GitHub page (Bui et al., 2016), but was written in Python2 and relies on legacy versions of several dependencies; we were unable to reproduce a suitable environment to try their code.

5 Empirical results

Here we entertain MC benchmarking exercises on two simulated examples and one real-world computer experiment. Code to re-produce all results (including for competitors) is available on our public GitHub repository: <https://bitbucket.org/gramacylab/deepgp-ex/>. We include the following comparators:

- DGP VEC: our Vecchia-DGP, via `deepgp` using defaults, Matèrn $\nu = 5/2$ kernel, independent predictions, and “warped” conditioning sets. See Section 4.1.
- DGP FULL: full, un-approximated analog of DGP VEC, with everything otherwise identical (also via `deepgp`). This comparator was not feasible for all data sizes.
- DGP DSVI: from Salimbeni and Deisenroth (2017), implemented in `gpflux`, with Matèrn $\nu = 5/2$ kernel. We follow package examples in using 100 k -means located inducing points. For numerical stability we required `eps = 1e-4`, lower bounding the noise parameter.

- DGP HMC: from [Havasi et al. \(2018\)](#), again using 100 inducing points. This code only supports a squared exponential kernel and estimates (i.e., does not fix) the noise parameter (g/ϵ_{ps}). We found no easy way to adjust these specifications, so we let them be.
- GP: stationary un-approximated Gaussian process following Eq. (3) with Matérn $\nu = 5/2$ kernel and anisotropic lengthscales estimated through MLE. This comparator was not feasible for all data sizes.
- GP SVEC: scaled Vecchia-GP of [Katzfuss et al. \(2020b\)](#), via `GPvecchia` and `GpGp`. This is a fast “shallow” GP where kernel hyperparameters are estimated (11) via lengthscales-adjusted conditioning sets. We use $m = 25$, Matérn $\nu = 5/2$ kernel, and independent predictions to match DGP VEC.

All DGP variations are restricted to two layers. Our metrics include out-of-sample root mean squared error (RMSE) and continuous rank probability score (CRPS; [Gneiting and Raftery, 2007](#)). Definitions are provided in Supp. B. Lower is better for both. While RMSE focuses on accuracy of predictive means, CRPS incorporates point-wise predictive variances, thus providing insight into UQ. Although our DGP VEC is able to provide full predictive covariance, our competitors DGP DSVI, DGP HMC, and GP SVEC cannot. Computation times are reported in Supp. F.

5.1 Simulated examples

Schaffer Function. The two-dimensional “fourth” Schaffer function (Supp. A.1) can be found in the Virtual Library of Simulation Experiments (VLSE; [Surjanovic and Bingham, 2013](#)). We follow the second variation therein using $X \in [-2, 2]^2$. The function is characterized by steep curved inclines followed by immediate drops. These quick turns are challenging for stationary GPs, making the Schaffer function an excellent candidate for DGPs. We fit models to Latin hypercube samples (LHS; [Mckay et al., 1979](#)) of training sizes $n \in \{100, 500, 1000\}$ with fixed noise $g = 10^{-8}$. We use LHS testing sets of size $n_p = 500$.

Results for 20 MC repetitions – all stochastic components from training/testing re-randomized – are displayed in Figure 4. All variations of our DGP fits outperform competitors by both metrics. Crucially,

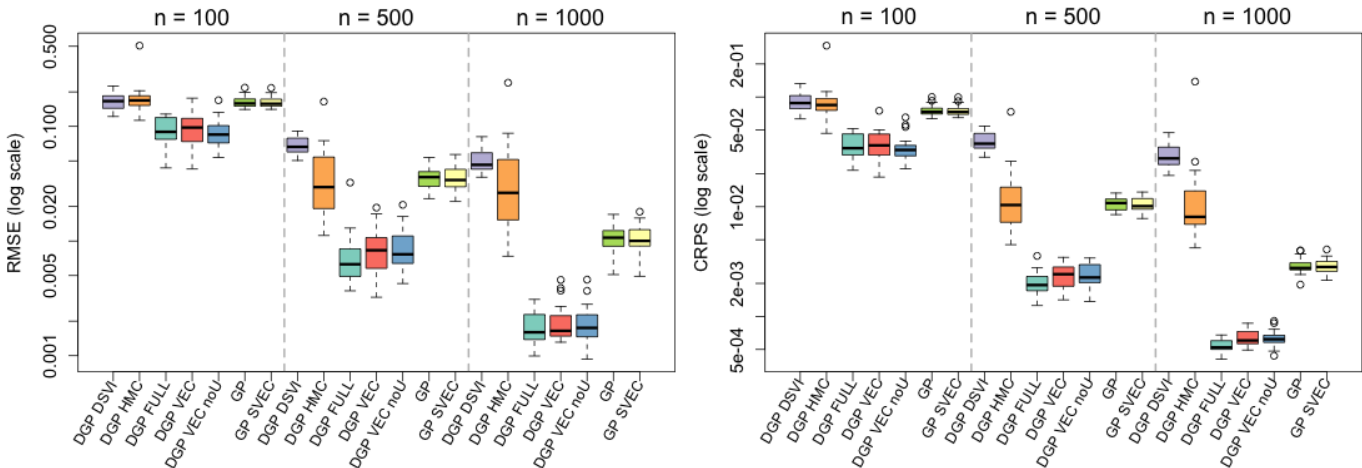


Figure 4: RMSE (left) and CRPS (right) on log scales for fits to the 2d Schaffer function as training size (n) increases. Boxplots represent the spread of 20 MC repetitions.

our Vecchia-DGP (DGP VEC) matches the performance of the un-approximated DGP (DGP FULL). For this example we additionally implemented a “DGP VEC noU” comparator, identical to DGP VEC but

without ordering/conditioning sets reset after pre-burn-in. Observe that this additional work is of dubious benefit empirically. Aside from MC variability, DGP VEC matches DGP VEC noU. Going forward we shall drop DGP VEC noU, focusing on our preferred DGP VEC setup, without evidence that results are better or worse and despite the additional (marginal) cost. Additional discussion is deferred to Section 6. Finally, at the outset we expected the stationary GPs (GP and GP SVEC) to perform poorly given the complexity of the response surface, but were surprised to see them holding their own against DGP HMC, and eventually surpassing it with $n = 1000$. We suspect this is a consequence of “blurry” inducing point approximations. The Vecchia approximated GP (GP SVEC) matched the performance of the full GP. Further study of the choice of conditioning set size m for both GPs and DGPs is provided in Supp. D.

G-function. The G-function (Marrel et al., 2009, Supp. A.2), also in the VLSE, is defined in arbitrary dimension. We worked with $d = 2$ in Figures 1 and 2. Here, we expand to $d = 4$. Higher dimensionality raises modeling challenges and demands larger training sets. We fit models to LHS samples of training sizes $n \in \{3000, 5000, 7000\}$ with fixed noise $g = 10^{-8}$. LHS testing sets were of size $n_p = 5000$. Results for 20 MC repetitions are displayed in Figure 5. Variations upon this setup with stochastic noise and higher input dimension, yielding similar results, are provided in Supp. E.

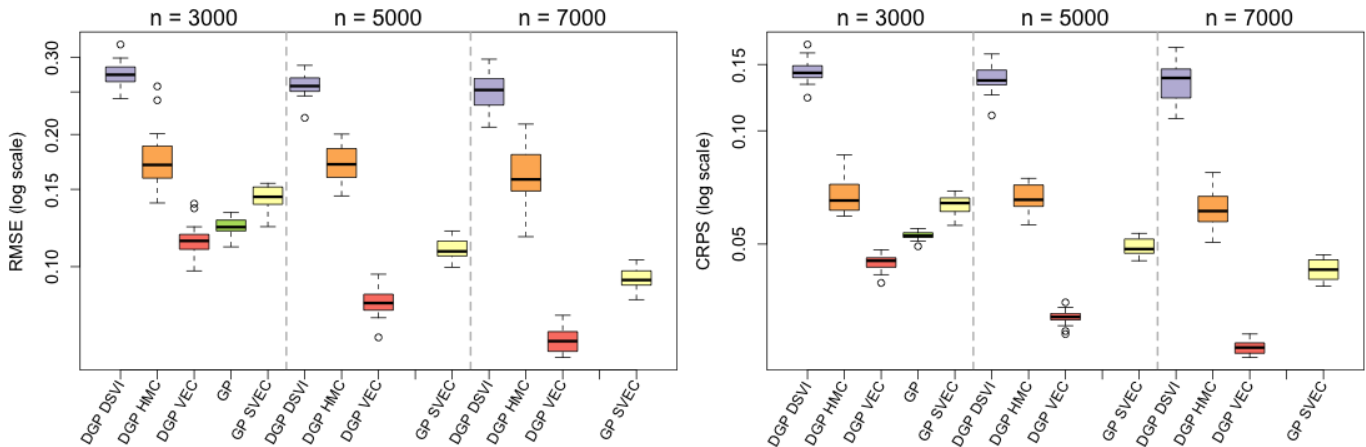


Figure 5: RMSE (left) and CRPS (right) on log scales for the 4d G-function.

Again, our DGP VEC outperforms both deep and shallow competitors. DGP HMC, aided by its ability to estimate hyperparameters, bests DGP DSVI, but neither benefits from additional training data. Their predictive capability appears to saturate; again, we suspect inducing points are to blame. While it is possible to increase the number of inducing points and potentially improve things, this requires adjustments to the source code and, in our experience, yields only marginal improvements before computation becomes prohibitive. GP SVEC is able to adapt to larger training sizes and surpass these deeper models. Our DGP VEC benefits from estimation of hyperparameters, additional depth, and learning from additional training data. While the full GP was not feasible for larger sample sizes, it significantly outperformed its Vecchia approximated GP counterpart but was not able to catch the non-stationary DGP VEC.

5.2 Satellite drag simulation

The *Test Particle Monte Carlo (TPM)* simulator (Mehta et al., 2014) models the bombardment of satellites in low earth orbit by atmospheric particles, returning coefficients of drag based on particle composition and input variables specifying satellite configuration. Researchers at Los Alamos National Lab, who developed

TPM, wished to build a surrogate achieving less than 1% prediction error (measured in root mean squared percentage error, RMSPE, Supp. B) with as few runs of the simulator as possible. Sun et al. (2019) used locally approximated GPs to reach the 1% goal with one million training data points. Later, Katzfuss et al. (2020b) achieved lower RMSPE’s using scaled Vecchia-GPs (GP SVEC). Here, we show that our Vecchia-DGP is able to beat the 1% RMSPE benchmark with as few as $n = 50,000$ (and can beat it consistently with $n = 100,000$), and provide better UQ than the stationary GP SVEC alternative.

We work specifically with the GRACE satellite, specified by a seven-dimensional input configuration, and a pure Helium atmospheric composition. For training data, we use random samples from Sun et al. (2019)’s one million runs in sizes of $n \in \{10000, 50000, 100000\}$. We use random out-of-sample testing sets of size $n_p = 50,000$ from the complement, and follow Sun et al. (2019) in fixing $g = 10^{-4}$. TPM simulations are technically stochastic, but the noise is very small.

In light of these large training data sizes and the accompanying computational burden, we make some strategic choices to initialize our DGP models and set up the MCMC for faster burn-in. First, we scale the seven input variables using estimated vectorized length-scales from GP SVEC (e.g. $X_i/\sqrt{\theta_i}$). This “pre-scaling” is common in computer surrogate modeling (e.g. Wycoff et al., 2021), and mirrors the “scaled” component of the GP SVEC model. Second, we “seed” our MCMC by first running a long, thoroughly burned-in, set of iterations for one sample of $n = 10,000$ and using the burned-in samples from this fit to initialize the chains for the larger data sets. This isn’t necessary in practice but helps reduce the burden of repeated applications in a MC benchmarking context.

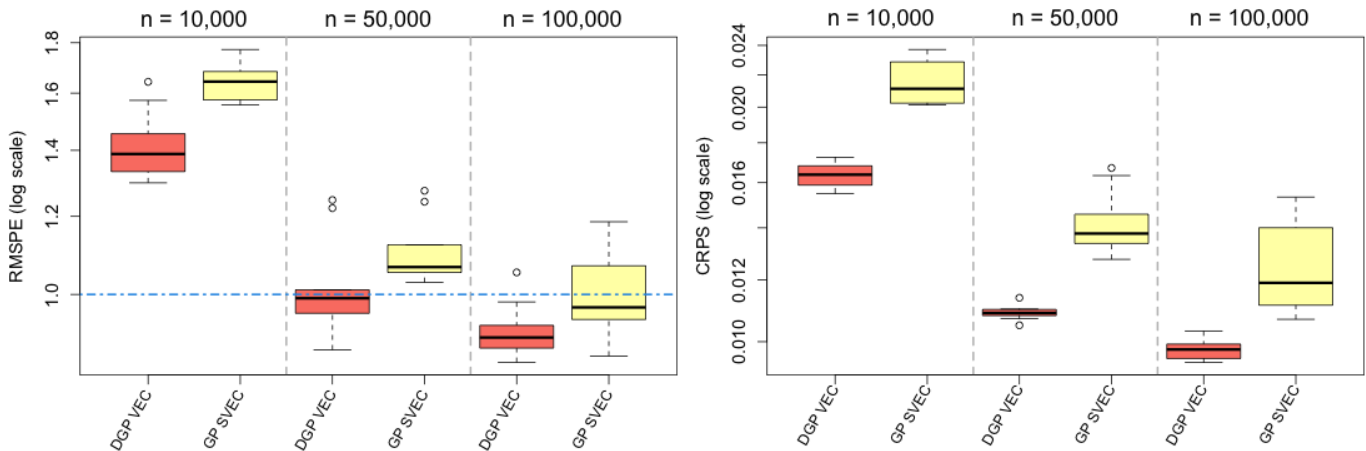


Figure 6: RMPSE (left) and CRPS (right) on log scales for fits to the satellite drag simulation. DGP DSVI and DGP HMC are omitted (with RMSPE’s between 30-35%). Horizontal line marks 1% RMSPE goal.

Results for 10 MC repetitions are displayed in Figure 6. Observe that DGP DSVI and DGP HMC results are omitted from these plots. Because they were not competitive (each producing RMSPE’s between 30-35%), their inclusion would severely expand the y -axis of the plots and render them hard to read. Our DGP VEC consistently outperforms the shallow/stationary GP SVEC and is able to achieve the 1% RMSPE goal with as few as 50,000 training observations. Compared to GP SVEC counterparts (with matched training/testing data), DGP VEC models have lower CRPS in all 30 MC repetitions (represented by 3 boxplots of 10) and lower RMSPE in 28 of the 30.

6 Discussion

In this work we have extended the capabilities of full posterior inference for deep Gaussian processes (DGPs) through the Vecchia approximation. DGPs offer more flexibility than shallow GPs as they are able to accommodate non-stationarity through the warpings of latent Gaussian layers. But inference is slow owing to cubic matrix decomposition. With a Vecchia approximation at each Gaussian layer, our fully-Bayesian DGP enjoys computational costs scaling linearly-in- n . We demonstrated the superior UQ and predictive power of Vecchia-DGPs over both approximate DGP competitors and stationary GPs.

We envision many opportunities for extension. Most notably, we restricted our simulation studies to those where the noise parameter (g) was fixed to a small value. While many computer simulations are deterministic, others are increasingly stochastic in nature (Baker et al., 2022) and prompt estimation of this hyperparameter, and possibly others. Our `deepgp` software is capable of estimating g through additional Metropolis steps. In the Vecchia context, our implementation incorporates the g parameter directly into the kernel by adding it to the diagonal of $\Sigma(x_i)$ and $\Sigma(X_{c(i)})$ in Eq. (7). Thus g is subsumed into $B_i(W)$ and $\sigma_i^2(W)$ which in turn populate U_w (9). As a demonstration of this capability, we provide a noisy simulated example in Supp. E. Results are very similar to those of Figure 5; our Vecchia-DGP outperforms across the board. Some authors separate responses into “true/latent” and “actual/observed” variables and caution against incorporating the noise parameter directly into the kernel (e.g. Katzfuss and Guinness, 2021; Datta et al., 2016), but we have not seen any drawbacks to our simplified approach in the DGP context. Furthermore, it may be possible to extend our DGP model to accommodate heteroskedastic noise through additional latent Gaussian random variables (Binois et al., 2018), although we caution that a model that is too flexible may fall prey to a signal–noise identifiability trap. One remedy is to provide for replicates in the design (Binois et al., 2019).

We restricted our empirical studies to a conditioning set size of $m = 25$, after finding limited advantage to larger m . [Supp. D explores varying m .] This echoes other GP-Vecchia works which have found success with small conditioning sets (e.g. Datta et al., 2016; Katzfuss et al., 2020b; Wu et al., 2022; Stroud et al., 2017). However, the size of m may be more important in larger dimensional problems. It may also be advantageous to use larger m for prediction, as it is otherwise rather cheaper than training. Similarly, we entertained only two-layer DGPs. Our experience with three-layer DGPs for surrogate modeling is that one of the latent layers settles into a near identity mapping, resulting in a lot more computation for little gain. In some cases, the added flexibility of a three-layer DGP can lead to overfitting and adversely affect predictions/UQ (Sauer et al., 2022). Our test functions and real-data computer simulations may not be non-stationary enough to warrant two or more levels of warping.

Perhaps the most intriguing extension lies in the choice of the Vecchia ordering and conditioning sets. Common practice, as we embraced, involves simply fixing an ordering and conditioning, sometimes informed by the data as when NNs are scaled or warped. Many works have investigated the effects of different ordering/conditioning structures (e.g. Katzfuss and Guinness, 2021; Guinness, 2018; Stein et al., 2004), yet these analyses have all been *post hoc*. If we view the ordering and conditioning structure as components of the stochastic (data generating) process, there may be potential to *learn* these, either through maximization or similar MCMC sampling. In our simulation studies, updating the NN conditioning sets based on learned latent warpings did not affect posterior predictions, perhaps suggesting that inference for these would have similar null-effects. Yet we suspect this is because the learned latent warpings we have encountered tend to rotate and stretch inputs, resulting in minimal effects on the proximity of observations. We are continuing to “hunt” for examples where more flexible neighborhoods are valuable.

Acknowledgements

This work was supported by the U.S. Department of Energy, Office of Science, Office of Advanced Scientific Computing Research and Office of High Energy Physics, Scientific Discovery through Advanced Computing (SciDAC) program under Award Number 0000231018.

References

- Baker, E., Barbillon, P., Fadikar, A., Gramacy, R. B., Herbei, R., Higdon, D., Huang, J., Johnson, L. R., Ma, P., Mondal, A., et al. (2022). “Analyzing stochastic computer models: A review with opportunities.” *Statistical Science*, 37, 1, 64–89.
- Banerjee, S., Gelfand, A. E., Finley, A. O., and Sang, H. (2008). “Gaussian predictive process models for large spatial data sets.” *Journal of the Royal Statistical Society. Series B: Statistical Methodology*, 70, 4, 825–848.
- Barnett, S. (1979). *Matrix Methods for Engineers and Scientists*. McGraw-Hill.
- Bates, D. and Maechler, M. (2021). *Matrix: Sparse and Dense Matrix Classes and Methods*. R package version 1.3-4.
- Betancourt, M. (2017). “A conceptual introduction to Hamiltonian Monte Carlo.” *arXiv preprint arXiv:1701.02434*.
- Binois, M., Gramacy, R. B., and Ludkovski, M. (2018). “Practical heteroscedastic gaussian process modeling for large simulation experiments.” *Journal of Computational and Graphical Statistics*, 27, 4, 808–821.
- Binois, M., Huang, J., Gramacy, R. B., and Ludkovski, M. (2019). “Replication or exploration? Sequential design for stochastic simulation experiments.” *Technometrics*, 61, 1, 7–23.
- Bui, T., Hernández-Lobato, D., Hernandez-Lobato, J., Li, Y., and Turner, R. (2016). “Deep Gaussian processes for regression using approximate expectation propagation.” In *International conference on machine learning*, 1472–1481. PMLR.
- Cole, D. A., Christianson, R. B., and Gramacy, R. B. (2021). “Locally induced Gaussian processes for large-scale simulation experiments.” *Statistics and Computing*, 31, 3, 1–21.
- Cutajar, K., Bonilla, E. V., Michiardi, P., and Filippone, M. (2017). “Random feature expansions for deep Gaussian processes.” In *International Conference on Machine Learning*, 884–893. PMLR.
- Damianou, A. and Lawrence, N. D. (2013). “Deep gaussian processes.” In *Artificial intelligence and statistics*, 207–215. PMLR.
- Datta, A. (2021). “Sparse Cholesky matrices in spatial statistics.” *arXiv preprint arXiv:2102.13299*.
- Datta, A., Banerjee, S., Finley, A. O., and Gelfand, A. E. (2016). “Hierarchical nearest-neighbor Gaussian process models for large geostatistical datasets.” *Journal of the American Statistical Association*, 111, 514, 800–812.
- Ding, L., Tuo, R., and Shahrampour, S. (2021). “A Sparse Expansion For Deep Gaussian Processes.” *arXiv preprint arXiv:2112.05888*.

- Domingues, R., Michiardi, P., Zouaoui, J., and Filippone, M. (2018). “Deep Gaussian Process autoencoders for novelty detection.” *Machine Learning*, 107, 8, 1363–1383.
- Dunlop, M. M., Girolami, M. A., Stuart, A. M., and Teckentrup, A. L. (2018). “How deep are deep Gaussian processes?” *Journal of Machine Learning Research*, 19, 54, 1–46.
- Dutordoir, V., Salimbeni, H., Hambro, E., McLeod, J., Leibfried, F., Artemev, A., van der Wilk, M., Hensman, J., Deisenroth, M. P., and John, S. (2021). “GPflux: A library for deep Gaussian processes.” *arXiv preprint arXiv:2104.05674*.
- Eddelbuettel, D. and Sanderson, C. (2014). “RcppArmadillo: Accelerating R with high-performance C++ linear algebra.” *Computational Statistics and Data Analysis*, 71, 1054–1063.
- Emery, X. (2009). “The kriging update equations and their application to the selection of neighboring data.” *Computational Geosciences*, 13, 3, 269–280.
- Finley, A., Sang, H., Banerjee, S., and Gelfand, A. (2009). “Improving the performance of predictive process modeling for large datasets.” *Computational Statistics & Data Analysis*, 53, 8, 2873–2884.
- Finley, A. O., Datta, A., and Banerjee, S. (2020). “spNNGP: R package for Nearest Neighbor Gaussian Process models.” *Journal of Statistical Software*.
- Finley, A. O., Datta, A., Cook, B. D., Morton, D. C., Andersen, H. E., and Banerjee, S. (2019). “Efficient algorithms for Bayesian nearest neighbor Gaussian processes.” *Journal of Computational and Graphical Statistics*, 1–14.
- Garton, N., Niemi, J., and Carriquiry, A. (2020). “Knot selection in sparse Gaussian processes with a variational objective function.” *Statistical Analysis and Data Mining: The ASA Data Science Journal*, 324–336.
- Gelman, A., Carlin, J. B., Stern, H. S., Dunson, D. B., Vehtari, A., and Rubin, D. B. (2013). *Bayesian Data Analysis*. CRC Press.
- Gneiting, T. and Raftery, A. E. (2007). “Strictly proper scoring rules, prediction, and estimation.” *Journal of the American statistical Association*, 102, 477, 359–378.
- Gramacy, R. B. (2020). *Surrogates: Gaussian Process Modeling, Design and Optimization for the Applied Sciences*. Boca Raton, Florida: Chapman Hall/CRC. <http://bobby.gramacy.com/surrogates/>.
- Gramacy, R. B. and Apley, D. W. (2015). “Local Gaussian process approximation for large computer experiments.” *Journal of Computational and Graphical Statistics*, 24, 2, 561–578.
- Gramacy, R. B. and Lee, H. K. H. (2008). “Bayesian treed Gaussian process models with an application to computer modeling.” *Journal of the American Statistical Association*, 103, 483, 1119–1130.
- Guinness, J. (2018). “Permutation and grouping methods for sharpening Gaussian process approximations.” *Technometrics*, 60, 4, 415–429.
- (2021). “Gaussian process learning via Fisher scoring of Vecchia’s approximation.” *Statistics and Computing*, 31, 3, 1–8.
- Guinness, J., Katzfuss, M., and Fahmy, Y. (2021). *GpGp: Fast Gaussian Process Computation Using Vecchia’s Approximation*. R package version 0.4.0.

- Hastings, W. K. (1970). “Monte Carlo sampling methods using Markov chains and their applications.” *Biometrika*, 57, 1, 97–109.
- Havasi, M., Hernández-Lobato, J. M., and Murillo-Fuentes, J. J. (2018). “Inference in deep Gaussian processes using stochastic gradient Hamiltonian Monte Carlo.” *Advances in neural information processing systems*, 31.
- Heaton, M. J., Datta, A., Finley, A. O., Furrer, R., Guinness, J., Guhaniyogi, R., Gerber, F., Gramacy, R. B., Hammerling, D., Katzfuss, M., et al. (2019). “A case study competition among methods for analyzing large spatial data.” *Journal of Agricultural, Biological and Environmental Statistics*, 24, 3, 398–425.
- Johnson, L. (2008). “Microcolony and Biofilm Formation as a Survival Strategy for Bacteria.” *Journal of Theoretical Biology*, 251, 24–34.
- Jones, D., Schonlau, M., and Welch, W. (1998). “Efficient global optimization of expensive black-box functions.” *Journal of Global Optimization*, 13, 4, 455–492.
- Kang, M. and Katzfuss, M. (2021). “Correlation-based sparse inverse Cholesky factorization for fast Gaussian-process inference.” *arXiv preprint arXiv:2112.14591*.
- Katzfuss, M. and Guinness, J. (2021). “A general framework for Vecchia approximations of Gaussian processes.” *Statistical Science*, 36, 1, 124–141.
- Katzfuss, M., Guinness, J., Gong, W., and Zilber, D. (2020a). “Vecchia approximations of Gaussian-process predictions.” *Journal of Agricultural, Biological and Environmental Statistics*, 25, 3, 383–414.
- Katzfuss, M., Guinness, J., and Lawrence, E. (2020b). “Scaled Vecchia approximation for fast computer-model emulation.” *arXiv preprint arXiv:2005.00386*.
- Katzfuss, M., Jurek, M., Zilber, D., and Gong, W. (2020c). *GPvecchia: Scalable Gaussian-Process Approximations*. R package version 0.1.3.
- Kaufman, C., Bingham, D., Habib, S., Heitmann, K., and Frieman, J. (2011). “Efficient emulators of computer experiments using compactly supported correlation functions, with an application to cosmology.” *The Annals of Applied Statistics*, 5, 4, 2470–2492.
- Kennedy, M. and O’Hagan, A. (2001). “Bayesian calibration of computer models.” *Journal of the Royal Statistical Society: Series B (Statistical Methodology)*, 63, 3, 425–464.
- Kim, H., Mallick, B., and Holmes, C. (2005). “Analyzing nonstationary spatial data using piecewise Gaussian processes.” *Journal of the American Statistical Association*, 100, 470, 653–668.
- Kita, H., Taniguchi, K., and Nakajima, Y. (2016). *Realistic Simulation of Financial Markets: Analyzing Market Behaviors by the Third Mode of Science*, vol. 4. Springer.
- Laradji, I. H., Schmidt, M., Pavlovic, V., and Kim, M. (2019). “Efficient deep Gaussian process models for variable-sized inputs.” In *2019 International Joint Conference on Neural Networks (IJCNN)*, 1–7. IEEE.
- Lázaro-Gredilla, M., Quinonero-Candela, J., Rasmussen, C. E., and Figueiras-Vidal, A. R. (2010). “Sparse spectrum Gaussian process regression.” *The Journal of Machine Learning Research*, 11, 1865–1881.

- Lin, L., Bingham, D., Broekgaarden, F., and Mandel, I. (2021). “Uncertainty quantification of a computer model for binary black hole formation.” *The Annals of Applied Statistics*, 15, 4, 1604–1627.
- Liu, H., Ong, Y.-S., Shen, X., and Cai, J. (2020a). “When Gaussian process meets big data: A review of scalable GPs.” *IEEE transactions on neural networks and learning systems*, 31, 11, 4405–4423.
- Liu, K., Li, Y., Hu, X., Lucu, M., and Widanage, W. D. (2020b). “Gaussian Process Regression With Automatic Relevance Determination Kernel for Calendar Aging Prediction of Lithium-Ion Batteries.” *IEEE Transactions on Industrial Informatics*, 16, 6, 3767–3777.
- Liu, X. and Guillas, S. (2017). “Dimension reduction for Gaussian process emulation: An application to the influence of bathymetry on tsunami heights.” *SIAM/ASA Journal on Uncertainty Quantification*, 5, 1, 787–812.
- Marmin, S. and Filippone, M. (2022). “Deep Gaussian Processes for Calibration of Computer Models.” *Bayesian Analysis*, 1 – 30.
- Marrel, A., Iooss, B., Laurent, B., and Roustant, O. (2009). “Calculations of Sobol indices for the Gaussian process metamodel.” *Reliability Engineering & System Safety*, 94, 3, 742–751.
- Mckay, D., Beckman, R., and Conover, W. (1979). “A Comparison of Three Methods for Selecting Vales of Input Variables in the Analysis of Output From a Computer Code.” *Technometrics*, 21, 239–245.
- Mehta, P. M., Walker, A., Lawrence, E., Linares, R., Higdon, D., and Koller, J. (2014). “Modeling satellite drag coefficients with response surfaces.” *Advances in Space Research*, 54, 8, 1590–1607.
- Melkumyan, A. and Ramos, F. T. (2009). “A sparse covariance function for exact Gaussian process inference in large datasets.” In *Twenty-first international joint conference on artificial intelligence*.
- Ming, D. and Guillas, S. (2021). “Linked Gaussian Process Emulation for Systems of Computer Models Using Matérn Kernels and Adaptive Design.” *SIAM/ASA Journal on Uncertainty Quantification*, 9, 4, 1615–1642.
- Ming, D., Williamson, D., and Guillas, S. (2021). “Deep Gaussian Process Emulation using Stochastic Imputation.” *arXiv preprint arXiv:2107.01590*.
- Murray, I., Adams, R. P., and MacKay, D. J. C. (2010). “Elliptical slice sampling.” In *The Proceedings of the 13th International Conference on Artificial Intelligence and Statistics*, vol. 9 of *JMLR: W&CP*, 541–548. PMLR.
- Paciorek, C. and Schervish, M. (2003). “Nonstationary covariance functions for Gaussian process regression.” *Advances in neural information processing systems*, 16.
- Pamadi, B., Covell, P., Tartabini, P., and Murphy, K. (2004). “Aerodynamic characteristics and glide-back performance of Langley glide-back booster.” In *22nd Applied Aerodynamics Conference and Exhibit*, 5382.
- Park, C. and Apley, D. (2018). “Patchwork kriging for large-scale Gaussian process regression.” *The Journal of Machine Learning Research*, 19, 1, 269–311.
- Picheny, V. and Ginsbourger, D. (2013). “A nonstationary space-time Gaussian process model for partially converged simulations.” *SIAM/ASA Journal on Uncertainty Quantification*, 1, 57–78.

- Quinonero-Candela, J. and Rasmussen, C. E. (2005). “A unifying view of sparse approximate Gaussian process regression.” *The Journal of Machine Learning Research*, 6, 1939–1959.
- Rajaram, D., Puranik, T. G., Ashwin Renganathan, S., Sung, W., Fischer, O. P., Mavris, D. N., and Ramamurthy, A. (2021). “Empirical assessment of deep gaussian process surrogate models for engineering problems.” *Journal of Aircraft*, 58, 1, 182–196.
- Rasmussen, C. E. and Williams, C. K. I. (2005). *Gaussian Processes for Machine Learning*. Cambridge, Mass.: MIT Press.
- Rushdi, A., Swiler, L., Phipps, E., D’Elia, M., and Ebeida, M. (2017). “VPS: Voronoi piecewise surrogate models for high-dimensional data fitting.” *International Journal for Uncertainty Quantification*, 7, 1.
- Salimbeni, H. and Deisenroth, M. (2017). “Doubly stochastic variational inference for deep Gaussian processes.” *arXiv preprint arXiv:1705.08933*.
- Sampson, P. D. and Guttorp, P. (1992). “Nonparametric estimation of nonstationary spatial covariance structure.” *Journal of the American Statistical Association*, 87, 417, 108–119.
- Sauer, A. (2022). *deepgp: Sequential Design for Deep Gaussian Processes using MCMC*. R package version 1.0.0.
- Sauer, A., Gramacy, R. B., and Higdon, D. (2022). “Active learning for deep Gaussian process surrogates.” *Technometrics*, 0, 0, 1–15.
- Schmidt, A. M. and O’Hagan, A. (2003). “Bayesian inference for non-stationary spatial covariance structure via spatial deformations.” *Journal of the Royal Statistical Society: Series B (Statistical Methodology)*, 65, 3, 743–758.
- Snelson, E. and Ghahramani, Z. (2006). “Sparse Gaussian Processes using Pseudo-inputs.” *Advances in Neural Information Processing Systems 18*, 1257–1264.
- Stein, M. L. (1999). *Interpolation of spatial data*. Springer-Verlag.
- Stein, M. L., Chi, Z., and Welty, L. J. (2004). “Approximating likelihoods for large spatial data sets.” *Journal of the Royal Statistical Society: Series B (Statistical Methodology)*, 66, 2, 275–296.
- Stroud, J. R., Stein, M. L., and Lysen, S. (2017). “Bayesian and maximum likelihood estimation for Gaussian processes on an incomplete lattice.” *Journal of computational and Graphical Statistics*, 26, 1, 108–120.
- Sun, F., Gramacy, R. B., Haaland, B., Lawrence, E., and Walker, A. (2019). “Emulating satellite drag from large simulation experiments.” *SIAM/ASA Journal on Uncertainty Quantification*, 7, 2, 720–759.
- Surjanovic, S. and Bingham, D. (2013). “Virtual library of simulation experiments: test functions and datasets.” <http://www.sfu.ca/~ssurjano>.
- Vecchia, A. V. (1988). “Estimation and model identification for continuous spatial processes.” *Journal of the Royal Statistical Society: Series B (Methodological)*, 50, 2, 297–312.
- Wu, L., Pleiss, G., and Cunningham, J. (2022). “Variational Nearest Neighbor Gaussian Processes.” *arXiv preprint arXiv:2202.01694*.

- Wycoff, N., Binois, M., and Gramacy, R. B. (2021). “Sensitivity Prewarping for Local Surrogate Modeling.” *arXiv preprint arXiv:2101.06296*.
- Zammit-Mangion, A., Ng, T. L. J., Vu, Q., and Filippone, M. (2021). “Deep compositional spatial models.” *Journal of the American Statistical Association*, 1–22.
- Zhang, Y., Zhao, H., Hassinger, I., Brinson, L. C., Schadler, L. S., and Chen, W. (2015). “Microstructure reconstruction and structural equation modeling for computational design of nanodielectrics.” *Integrating Materials and Manufacturing Innovation*, 4, 1, 14.

SUPPLEMENTARY MATERIAL

A Simulation functions

A.1 Schaffer function

The two-dimensional ‘‘fourth’’ Schaffer function (Surjanovic and Bingham, 2013) is defined as

$$f(x_1, x_2) = 0.5 + \frac{\cos^2(\sin(|x_1^2 - x_2^2|)) - 0.5}{[1 + 0.001(x_1^2 + x_2^2)]^2}.$$

We use the restricted domain $X \in [-2, 2]^2$.

A.2 G-function

The G-function (Marrel et al., 2009) is defined in d -dimension over the unit cube $X \in [0, 1]^d$ as

$$f(\mathbf{x}) = \prod_{i=1}^d \frac{|4x_i - 2| + a_i}{1 + a_i} \quad \text{where} \quad a_i = \frac{i - 2}{2} \quad \text{for all} \quad i = 1, \dots, d.$$

B Performance metrics

B.1 Prediction error

Let μ^* represent posterior mean predictions at n_p testing locations. Let y^{true} represent the corresponding observed values. Root mean squared error (RMSE) and root mean squared prediction error (RMSPE) are respectively defined as

$$\text{RMSE} = \sqrt{\frac{1}{n_p} \sum_{i=1}^{n_p} ((\mu_i^* - y_i^{\text{true}})^2)} \quad \text{RMSPE} = \sqrt{\frac{1}{n_p} \sum_{i=1}^{n_p} \left(\left(100 * \frac{\mu_i^* - y_i^{\text{true}}}{y_i^{\text{true}}} \right)^2 \right)}$$

B.2 Uncertainty quantification

Given a Gaussian posterior predictive distribution with predicted mean μ^* and point-wise standard deviations σ^* , the continuous rank probability score (CRPS; Gneiting and Raftery, 2007) is defined as

$$\text{CRPS}(y^{\text{true}} | \mu^*, \sigma^*) = \frac{1}{n_p} \sum_{i=1}^{n_p} \left[\sigma_i^* \left(\frac{1}{\sqrt{\pi}} - 2\phi(z_i) - z_i(2 * \Phi(z_i) - 1) \right) \right] \quad \text{for} \quad z_i = \frac{y_i^{\text{true}} - \mu_i^*}{\sigma_i^*}$$

where ϕ is the standard Gaussian pdf and Φ is the standard Gaussian cdf.

C Derivations

C.1 Partitioned matrix inverse

The inverse of a partitioned matrix follows (Barnett, 1979):

$$\begin{bmatrix} A_{11} & A_{12} \\ A_{21} & A_{22} \end{bmatrix} = \begin{bmatrix} B_{11} & B_{12} \\ B_{21} & B_{22} \end{bmatrix}^{-1} \quad \text{where} \quad \begin{aligned} A_{11} &= (B_{11} - B_{12}B_{22}^{-1}B_{21})^{-1} \\ A_{12} &= -B_{11}^{-1}B_{12}(B_{22} - B_{21}B_{11}^{-1}B_{12})^{-1} \\ A_{21} &= -B_{22}^{-1}B_{21}(B_{11} - B_{12}B_{22}^{-1}B_{21})^{-1} \\ A_{22} &= (B_{22} - B_{21}B_{11}^{-1}B_{12})^{-1} \end{aligned}$$

C.2 Vecchia posterior predictive moments

We aim to predict \mathcal{Y} at locations \mathcal{W} conditioned on observed Y and W . We assume a zero-mean Gaussian process prior distribution,

$$\begin{bmatrix} Y \\ \mathcal{Y} \end{bmatrix} \sim \mathcal{N}_{n+n_p}(0, \Sigma_{\text{stack}}) \quad \text{where} \quad \Sigma_{\text{stack}} = \Sigma \left(\begin{bmatrix} W \\ \mathcal{W} \end{bmatrix} \right) = \begin{bmatrix} \Sigma(W) & \Sigma(W, \mathcal{W}) \\ \Sigma(\mathcal{W}, W) & \Sigma(\mathcal{W}) \end{bmatrix}.$$

Under the Vecchia-approximation, we decompose the precision matrix using the sparse upper-lower Cholesky decomposition, with entries populated according to (9),

$$U_{\text{stack}} = \begin{bmatrix} U_w & U_{w, \mathcal{W}} \\ 0 & U_{\mathcal{W}} \end{bmatrix} \quad \text{such that} \quad \Sigma_{\text{stack}} = \left(U_{\text{stack}} U_{\text{stack}}^\top \right)^{-1} = \left(\begin{bmatrix} U_w U_w^\top + U_{w, \mathcal{W}} U_{w, \mathcal{W}}^\top & U_{w, \mathcal{W}} U_{\mathcal{W}}^\top \\ U_{\mathcal{W}} U_{w, \mathcal{W}}^\top & U_{\mathcal{W}} U_{\mathcal{W}}^\top \end{bmatrix} \right)^{-1}.$$

We aim to find a closed-form solution to the posterior predictive moments (3),

$$\mathcal{Y} \mid Y, W \sim \mathcal{N}_{n_p}(\mu^*, \Sigma^*) \quad \text{for} \quad \begin{aligned} \mu^* &= \Sigma(\mathcal{W}, W) \Sigma(W)^{-1} Y \\ \Sigma^* &= \Sigma(\mathcal{W}) - \Sigma(\mathcal{W}, W) \Sigma(W)^{-1} \Sigma(W, \mathcal{W}), \end{aligned}$$

which can avoid dense covariance matrices by instead relying on elements of the sparse U_{stack} . The simplification of Σ^* follows directly from the partitioned matrix inverse (App. C.1),

$$U_{\mathcal{W}} U_{\mathcal{W}}^\top = \left(\Sigma(\mathcal{W}) - \Sigma(\mathcal{W}, W) \Sigma(W)^{-1} \Sigma(W, \mathcal{W}) \right)^{-1} \implies \Sigma^* = \left(U_{\mathcal{W}} U_{\mathcal{W}}^\top \right)^{-1}.$$

The calculation of μ^* first involves simplification of $\Sigma(W)$ and $\Sigma(\mathcal{W}, W)$, again using partitioned matrix inverses (App. C.1):

$$\begin{aligned} \Sigma(W) &= \left(U_w U_w^\top + U_{w, \mathcal{W}} U_{w, \mathcal{W}}^\top - U_{w, \mathcal{W}} U_{\mathcal{W}}^\top \left(U_{\mathcal{W}} U_{\mathcal{W}}^\top \right)^{-1} U_{\mathcal{W}} U_{w, \mathcal{W}}^\top \right)^{-1} \\ &= \left(U_w U_w^\top \right)^{-1} \\ \Sigma(\mathcal{W}, W) &= - \left(U_{\mathcal{W}} U_{\mathcal{W}}^\top \right)^{-1} U_{\mathcal{W}} U_{w, \mathcal{W}}^\top \left(U_w U_w^\top + U_{w, \mathcal{W}} U_{w, \mathcal{W}}^\top - U_{w, \mathcal{W}} U_{\mathcal{W}}^\top \left(U_{\mathcal{W}} U_{\mathcal{W}}^\top \right)^{-1} U_{\mathcal{W}} U_{w, \mathcal{W}}^\top \right)^{-1} \\ &= - \left(U_{\mathcal{W}} U_{\mathcal{W}}^\top \right)^{-1} U_{\mathcal{W}} U_{w, \mathcal{W}}^\top \left(U_w U_w^\top \right)^{-1}. \end{aligned}$$

Together, these yield

$$\begin{aligned} \mu^* &= \Sigma(\mathcal{W}, W) \Sigma(W)^{-1} Y \\ &= - \left(U_{\mathcal{W}} U_{\mathcal{W}}^\top \right)^{-1} U_{\mathcal{W}} U_{w, \mathcal{W}}^\top \left(U_w U_w^\top \right)^{-1} U_w U_w^\top Y \\ &= - \left(U_{\mathcal{W}}^\top \right)^{-1} U_{w, \mathcal{W}}^\top Y. \end{aligned}$$

D Conditioning set size

Here we evaluate Vecchia-DGP (DGP VEC) and scaled Vecchia-GP (GP SVEC) models on the two-dimensional Schaffer function while varying the conditioning set size, m . The set-up is identical to that of Section 5.1, with the exception that we worked with $n = 1,000$ and $m \in \{5, 10, 25, 50, 100\}$. Resulting RMSE and CRPS from 20 MC repetitions are shown in Figure 7.

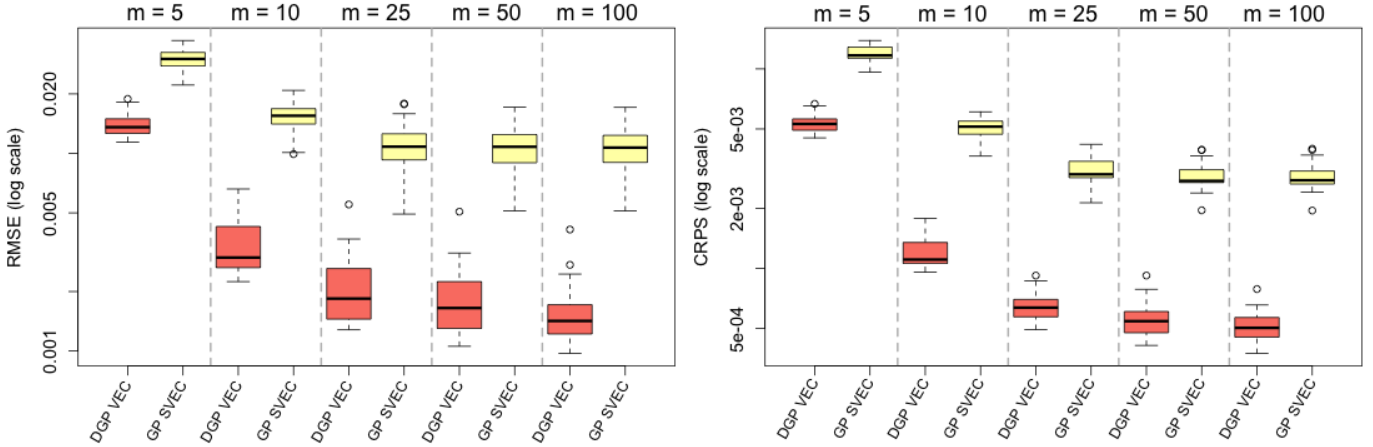


Figure 7: RMSE (left) and CRPS (right) for fits to the 2d Schaffer function as conditioning set size (m) increases (same m used for training and prediction). Boxplots represent the spread of 20 repetitions.

As expected, increasing the size of the conditioning set improves predictive accuracy for both models. However, the benefits of conditioning on more points diminishes beyond $m = 25$. While present in both models, this “leveling off” effect appears more starkly in the stationary GP SVEC than the non-stationary DGP VEC. Table 1 reports computation time (in minutes on a 16-core hyperthreaded, Intel i9 CPU at 3.6GHz) for each model/ m configuration. The optimization-based inference of the GP SVEC model is fast enough that larger m do not incur additional computational costs, practically speaking. The sampling based nature of DGP VEC reveals the cubic costs of larger conditioning sets ($\mathcal{O}(nm^3)$). These cubic costs, and the minimal predictive improvements realized with larger m , motivate our choice of $m = 25$ for all other exercises and as the default setting in our software.

Model	$m = 5$	$m = 10$	$m = 25$	$m = 50$	$m = 100$
DGP VEC	3.16	4.19	8.91	25.80	92.09
GP SVEC	0.02	0.01	0.01	0.02	0.07

Table 1: Computation times in minutes for 2d Schaffer function exercise of Figure 7.

E Additional simulations

E.1 Simulation with noise

As an example of a noisy simulation, we re-create the Monte Carlo exercise for the G-function (Marrel et al., 2009) with the addition of additive Gaussian noise $\epsilon_i \sim \mathcal{N}(0, 0.01^2)$. The set-up is equivalent to that

of Section 5.1, except that each model is now tasked with estimating a noise parameter (i.e. `true.g = NULL` in `deepgp`). The DGP HMC and GP SVEC models have built-in capability to estimate noise. The DGP DSVI model does not, so we simply fix the noise parameter to the true variance ($g = 0.01$). To account for the extra challenge of distinguishing signal from noise, we double the data sizes to $n \in \{6000, 10000, 14000\}$ and $n_p = 10000$. Code to reproduce these results is available in our github repository.

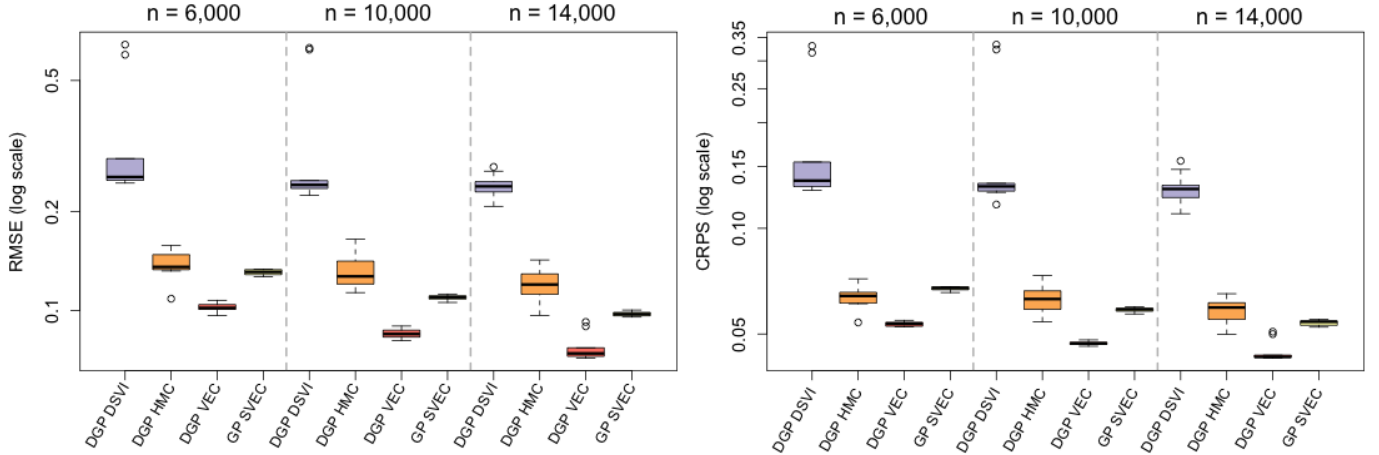


Figure 8: RMSE (left) and CRPS (right) on log scales for the 4d G-function observed with Gaussian white noise. Boxplots represent the spread of 10 MC repetitions.

The results resemble Figure 5, suggesting the addition of noise does not affect the comparative efficacy of the models. DGP HMC and GP SVEC perform similarly, the former benefiting from the flexibility of DGP layers and the latter benefiting from the Vecchia approximation (as compared to inducing points). The DGP VEC model outperforms across the board. When matched by training/testing data, DGP VEC had lower RMSE and CRPS than each of these comparators in 30/30 trials.

E.2 Higher dimensional simulation

To display functionality in higher dimension, we again re-create the Monte Carlo exercise for the G-function, this time expanding to $d = 6$. The set-up is equivalent to that of Section 5.1. Higher dimension demands larger data sizes; we entertain random LHS training designs of size $n \in \{10000, 20000, 30000\}$ and LHS testing designs of size $n_p = 20000$.

As in the lower dimensional exercises, DGP VEC outperforms on both prediction error and uncertainty quantification. Both DGP DSVI and DGP HMC are limited by inducing point approximations which are especially blurry in high dimensions. We note that the DGP HMC model is at a slight disadvantage since it estimates a noise parameter – the poor fits from this model may be over-estimating the noise.

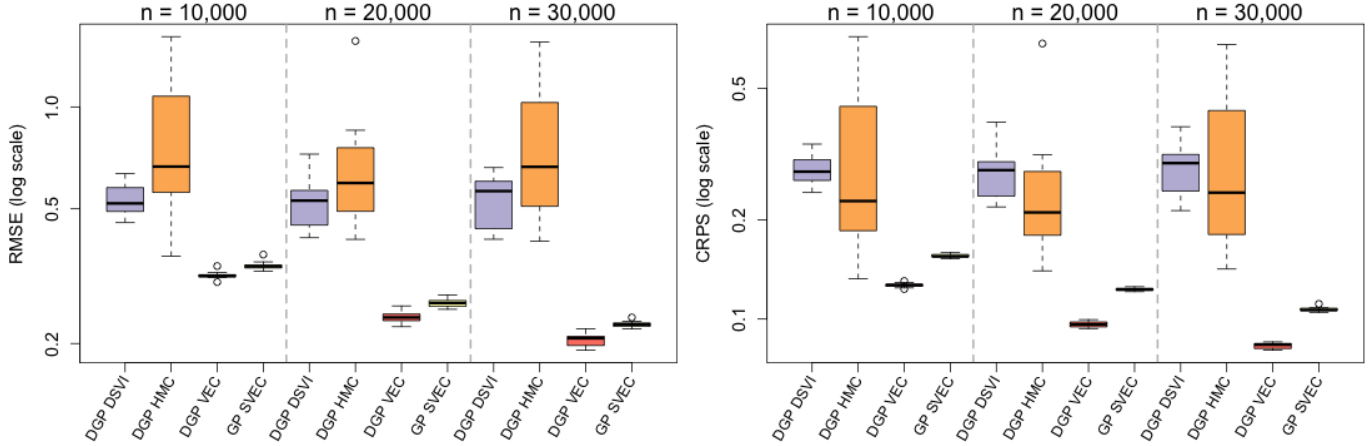


Figure 9: RMSE (left) and CRPS (right) on log scales for the 6d G-function. Boxplots represent the spread of 10 MC repetitions.

F Computation times

The following tables report computation times (in minutes) for the simulation exercises of Section 5 and Supp. E. We report the computation time for a single Monte Carlo exercise; times for each randomized trial are similar. All times were recorded on a 16-core hyperthreaded, Intel i9 CPU at 3.6GHz. The compute times of MCMC methods are directly tied to the number of MCMC samples collected. DGP VEC models sampled 3000 iterations for the Schaffer function, 3000 for the G-function, and 2000 for the satellite simulation. DGP HMC models utilized the default of 10,000 iterations. Un-approximated models (DGP FULL and GP) were not run for larger data sizes due to the cubic computational costs.

Model	N = 100	N = 500	N = 1,000
DGP DSVI	0.17	0.50	0.97
DGP HMC	0.58	1.45	2.43
DGP FULL	1.71	194.61	1605.94
DGP VEC	2.08	5.12	8.16
DGP VEC noU.	1.95	5.04	8.27
GP	0.03	0.55	3.48
GP SVEC	0.04	0.08	0.07

Table 2: Computation times in minutes for the Schaffer function exercises of Section 5.1 (Figure 4).

Model	N = 3,000	N = 5,000	N = 7,000
DGP DSVI	3.10	5.11	7.14
DGP HMC	7.59	12.21	17.35
DGP VEC	39.70	64.38	89.06
GP	807.33	N/A	N/A
GP SVEC	0.05	0.09	0.09

Table 3: Computation times in minutes for the G-function exercises of Section 5.1 (Figure 5).

Model	N = 10,000	N = 50,000	N = 100,000
DGP DSVI	12.00	59.13	109.20
DGP HMC	26.72	26.29	26.47
DGP VEC	190.57	809.75	1606.15
GP SVEC	0.17	0.18	0.18

Table 4: Computation times in minutes for the satellite simulation exercises of Section 5.2 (Figure 6).

Model	N = 6,000	N = 10,000	N = 14,000
DGP DSVI	6.15	10.17	14.22
DGP HMC	14.69	24.94	25.19
DGP VEC	84.85	132.41	179.44
GP SVEC	0.09	0.09	0.09

Table 5: Computation times in minutes for the noisy G-function exercise of Supp. E.1 (Figure 8).

Model	N = 10,000	N = 20,000	N = 30,000
DGP DSVI	11.73	21.82	35.04
DGP HMC	25.91	26.05	26.14
DGP VEC	235.49	425.43	623.89
GP SVEC	0.43	0.34	0.34

Table 6: Computation times in minutes for the 6d G-function exercise of Supp. E.2 (Figure 9).